ACS NANO
Cite This: ACS Nano 2019, 13, 9880–9894
www.acsnano.org

ARTICLE

An *in Vivo* miRNA Delivery System for Restoring Infarcted Myocardium

Huaxiao Yang,*[,†] Xulei Qin,[†] Huiyuan Wang,[‡] Xin Zhao,[†] Yonggang Liu,[†] Hung-Ta Wo,[†] Chun Liu,[†] Masataka Nishiga,[†] Haodong Chen,[†] Jing Ge,[§] Nazish Sayed,[†] Oscar J. Abilez,[†] Dan Ding,[∥] Sarah C. Heilshorn,[‡] and Kai Li*[,§,⊥]

[†]Stanford Cardiovascular Institute, Stanford University School of Medicine, Stanford, California 94305, United States
[‡]Department of Materials Science and Engineering, Stanford University, Stanford, California 94305, United States
[§]Department of Biomedical Engineering, Southern University of Science and Technology, Shenzhen, Guangdong 518055, China
[∥]State Key Laboratory of Medicinal Chemical Biology, Key Laboratory of Bioactive Materials, Ministry of Education, College of Life Sciences, Nankai University, Tianjin 300071, China
[⊥]Department of Radiology, Stanford University School of Medicine, Stanford, California 94305, United States

Supporting Information

ABSTRACT: **A major challenge in myocardial infarction (MI)-related heart failure treatment using microRNA is the efficient and sustainable delivery of miRNAs into myocardium to achieve functional improvement through stimulation of intrinsic myocardial restoration. In this study, we established an *in vivo* delivery system using polymeric nanoparticles to carry miRNA (miNPs) for localized delivery within a shear-thinning injectable hydrogel. The miNPs triggered proliferation of human embryonic stem cell-derived cardiomyocytes and endothelial cells (hESC-CMs and hESC-ECs) and promoted angiogenesis in hypoxic conditions, showing significantly lower cytotoxicity than Lipofectamine. Furthermore, one injected dose of hydrogel/miNP in MI rats demonstrated significantly improved cardiac functions: increased ejection fraction from 45% to 64%, reduced scar size from 20% to 10%, and doubled capillary density in the border zone compared to the control group at 4 weeks. As such, our results indicate that this injectable hydrogel/miNP composite can deliver miRNA to restore injured myocardium efficiently and safely.**

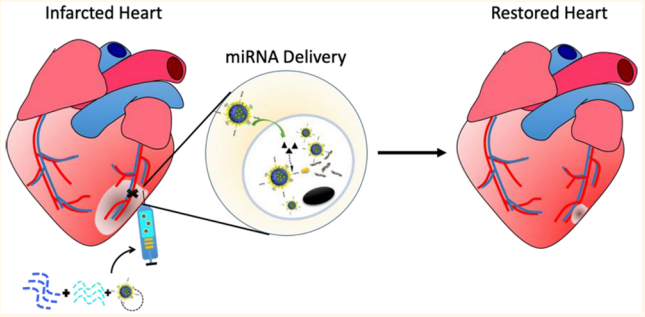

KEYWORDS: *cardiovascular disease, regenerative medicine, gene delivery, conjugated polymer, myocardial infarction*

According to the 2018 updated heart disease and stroke statistics released by the American Heart Association, more than 6.5 million Americans suffer from heart failure, with myocardial infarction (MI) being a leading cause.[1] MI is closely associated with coronary artery occlusion, which results in severe downstream cardiomyocyte (CM) death.[2] Current post-MI therapy options, including surgical interventions (*e.g.*, coronary angioplasty and stenting) and pharmacological treatments (*e.g.*, beta-blockers,[3] antiplatelet therapy,[4] and statin therapy),[5] are limited to mitigating symptoms and do not induce tissue repair. Although stem cell therapies promise the possibility of eventually repairing or regenerating the infarcted myocardium,[6−9] they have several limitations that impede their current use in clinical practice. These include low cell retention and engraftment, excessive cell dosing requirements, time-consuming cell preparation and maintenance, difficulties in storage and transportation, immune response upon allogeneic transplantation, and risk of tumorigenicity.[8,9]

To overcome these obstacles, new therapeutic approaches to deliver trophic factors and microRNAs (miRNAs) are being intensively studied. For instance, several miRNAs are involved in the cardiovascular repair or functional improvements of ischemic heart, including miR-1, miR-21, miR-199a-3p, miR-590-3p, and others.[10−14] Specifically, miR-199a-3p has shown great therapeutic potential to promote cardiovascular regeneration by stimulating proliferation of mouse/rat CMs *via* molecular targets of HOMER1 and CLIC5, and rat endothelial cells *via* caveolin-2.[15−17] It can also trigger cardioprotection from ischemic cardiomyopathy through carvedilol to activate p-AKT survival signaling,[18] and prevent lung/kidney fibrosis

Received: May 1, 2019
Accepted: May 31, 2019
Published: May 31, 2019

DOI: 10.1021/acsnano.9b03343
ACS Nano 2019, 13, 9880–9894

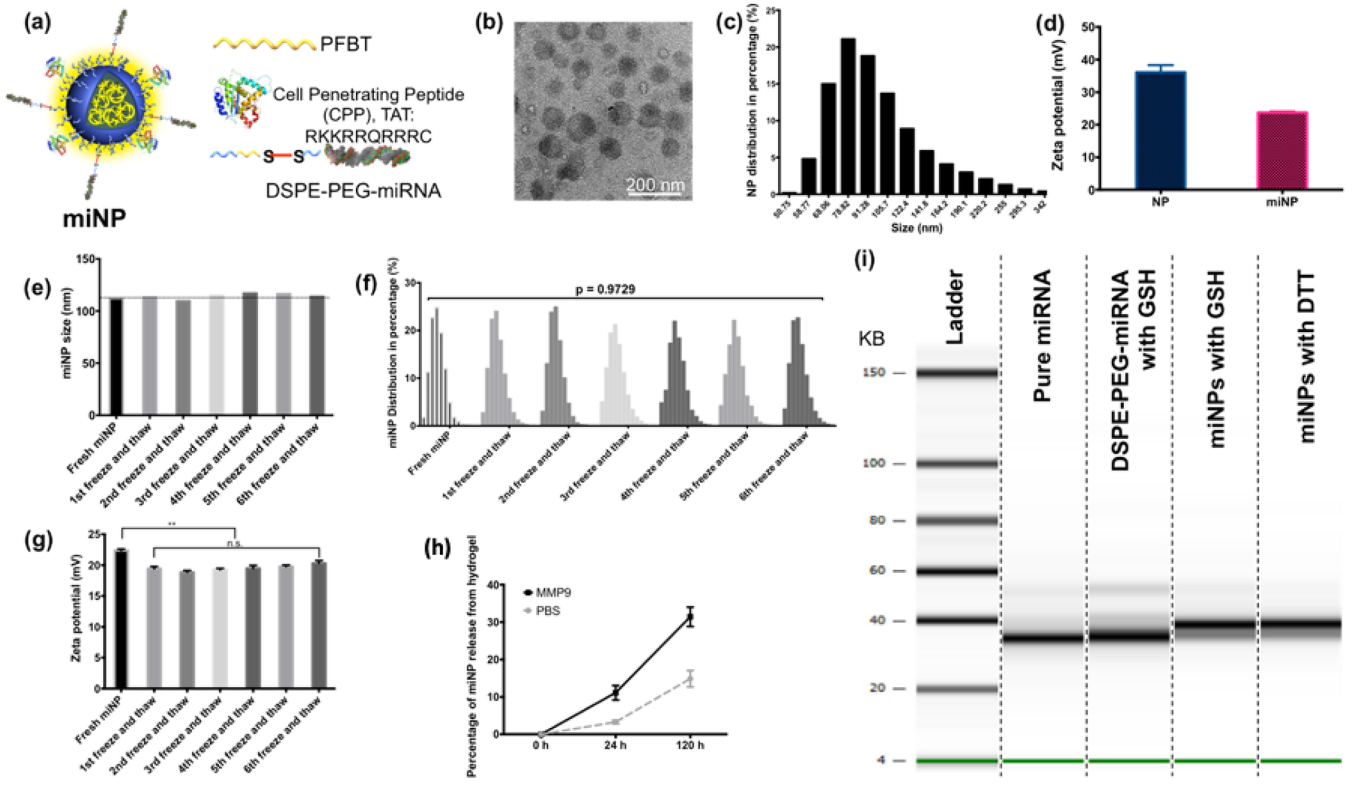

Figure 1. Characterization of miNPs and miRNA release from miNPs. (a) The animated structure of miNPs with a core−shell structure: PFBT core, PEG shell, and TAT and miR-199a-3p conjugate on the surface of NPs. (b) The TEM image of miNPs, scale bar = 200 nm. (c) The size distribution of fresh miNPs in percentages. (d) Zeta potentials of NPs with or without miRNAs. (e) Averaged sizes, (f) distribution in percentage, and (g) zeta potentials of miNPs before and after 6 cycles of freezing at −80 °C and thawing at room temperature ($p < 0.01$, n.s.: nonsignificant). (h) Percentage of miNP release from ELP-HA hydrogel with PBS or MMP-9, $n = 4$. (i) miRNA release from DSPE-PEG-miRNA conjugates by GSH cleavage and miNPs by GSH or DTT cleavage with the pure miRNA as a control.**

through suppressing TGFβ signaling on FGF7 and HGF.[19] To make gene therapy by miRNAs feasible for future clinical applications, several *in vivo* delivery approaches have been explored,[19] including the use of Adeno-associated virus (AAV) and lipocomplexes. For example, AAV packaging miR-199a-3p was intraperitoneally injected into neonatal and adult mice with MI to trigger the proliferation of CMs, restoring the function of the infarcted myocardium.[16] Although AAV has demonstrated very high *in vitro* and *in vivo* transfection efficiency in many cell and animal models, it is still clinically limited by concerns of potential immune response, expression of transgenes over prolonged periods, and lack of spatiotemporal controls.[20,21] Recently, AAV6-miR-199a was associated with sudden death of pigs at weeks 7−8 after one dose of injection.[22] On the other hand, lipocomplex-based gene delivery also has its own clinical limitations, including high cytotoxicity, low transfection efficiency, and instability in blood and serum.[15,23] As an alternative approach, polymeric nanoparticles (NPs) have the potential advantages of low cytotoxicity, high stability in blood, less severe immune responses, biodegradability, and controlled release. For example, polymeric NPs are increasingly being utilized as biological carriers for siRNA/miRNA delivery for several cancer treatments in clinical trials,[24,25] providing a promising basis for the development of RNA carriers to promote cardiac regeneration.

It is challenging to achieve localized NP/gene/drug delivery and transfection in the beating heart with spatial accuracy and high efficiency.[26] To overcome this barrier, we recently developed a highly efficient transfection approach for CMs using cell-penetrating peptides (CPPs) to greatly enhance NP uptake with minimum leakage.[27,28] The presence of protein transduction domains within CPPs enables the efficient transport of CPP-linked cargo into the cytoplasm, even at low concentrations.[25] Typically, localized delivery of therapeutics for MI involves an intramyocardial injection, either through interventional procedures or open chest surgery.[6,7] However, direct drug injection into the myocardium always results in low drug retention due to mechanical extrusion out of the beating cardiac tissue and rapid diffusion into adjacent tissue areas. In response, injectable hydrogels have been developed to release encapsulated drugs sustainably and locally,[29,30] with minimal interference on the cardiac electrical and mechanical functions.[31,32] Recently, we synthesized and characterized a family of protein-engineered hydrogels with shear-thinning viscosity and rapid self-healing back into a gel for minimally invasive intramyocardial injection with highly preserved drug and cell activities.[33−35]

In this study, a highly efficient and cardiovascular biocompatible *in vivo* miRNA delivery system was designed and applied in the treatment of post-MI in a rat ischemia/reperfusion model. Since miR-199a-3p has demonstrated the potential for the treatment of cardiovascular diseases, we chose it as our model miRNA in the *in vivo* delivery system. We used polymeric NPs as miRNA carriers (miNPs) together with a shear-thinning hydrogel to encapsulate the miNPs. This delivery system was used to achieve minimally invasive intramyocardial injection with localized miNP release and

DOI: 10.1021/acsnano.9b03343
ACS Nano 2019, 13, 9880−9894

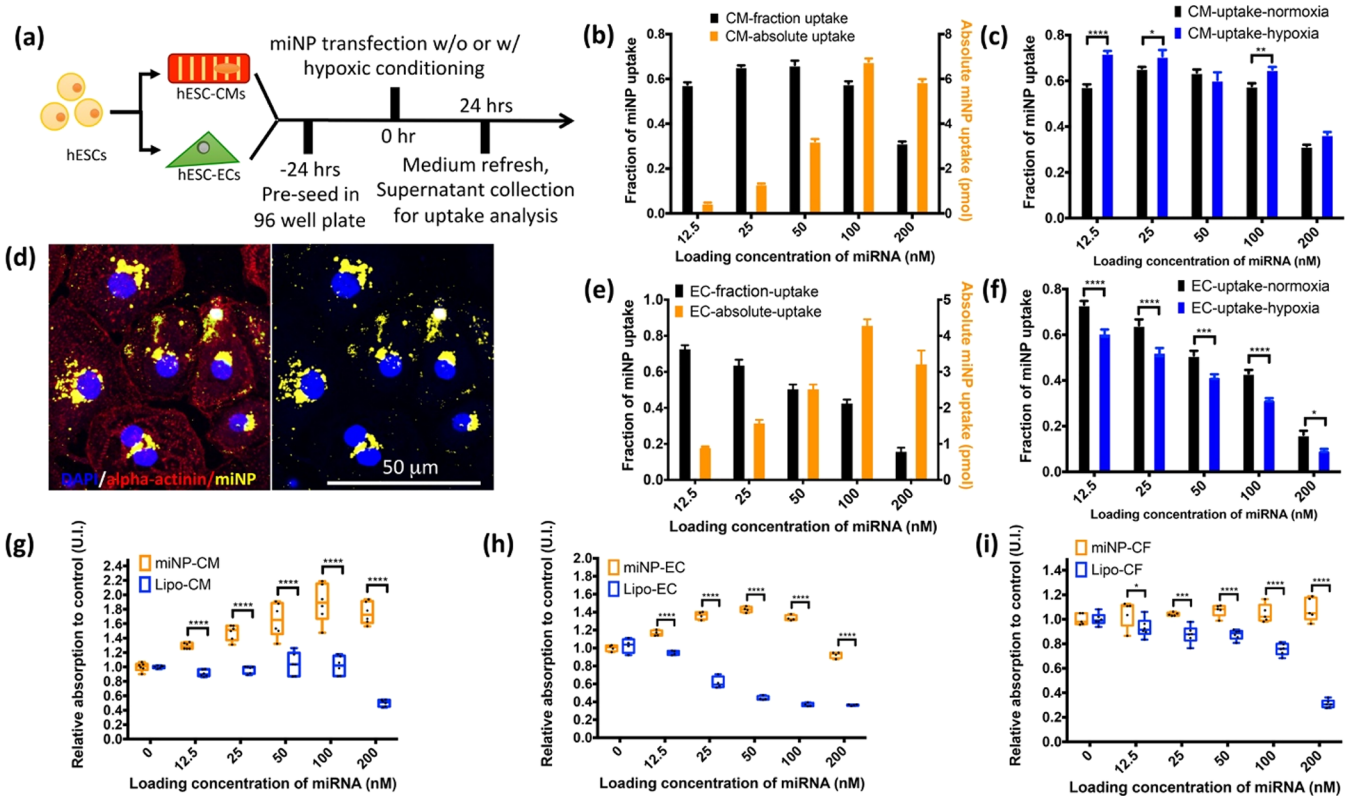

Figure 2. miNP uptake and cytotoxicity in the human cardiovascular cells. (a) Schematic procedures of miNP uptake sampling from the cardiovascular cells: hESC-CMs and hESC-ECs. (b) miNP uptake percentage and absolute amount in hESC-CMs. (c) miNP uptake percentage in hESC-CMs under normoxic or hypoxic condition. (d) Confocal images of miNPs (yellow) internalized in the hESC-CMs (fluorescently immunostained with alpha-actinin in red and DAPI in blue), scale bar: 50 μm. (e) miNP uptake percentage and absolute amount in hESC-ECs. (f) miNP uptake percentage in hESC-ECs under normoxic or hypoxic condition. (g,h,i) Cytotoxicity of miNP on the hESC-CMs, hESC-ECs, and hCFs at 48 h post-transfection with varied loading concentrations of miRNA using miNP or lipo as the delivery carriers, respectively. $N = 4-6$, $^{*}p < 0.05$, $^{**}p < 0.01$, $^{***}p < 0.001$, $^{****}p < 0.0001$.

interaction with CMs in the border zone, leading to significantly improved cardiac function with reduced scar size and enhanced capillary density. Furthermore, the molecular properties and biological functions of miNPs were tested and verified in an *in vitro* model of hESC-CMs and hESC-ECs in hypoxia.

RESULTS

Synthesis and Characterization of miNPs and miRNA Release. Three layers compose the structure of miNPs as presented in Figure 1a: (i) a fluorescent PFBT core to improve *in vivo* tracking, (ii) a DSPE-PEG shell to improve NP stability, and (iii) surface presence of miRNA and a CPP including the amino acid sequence TAT, to enhance the efficiency of miNP uptake. The miNPs were synthesized *via* three steps as shown in Figure S1 in the Supporting Information. First, miRNA was covalently linked to one end of a DSPE-PEG chain *via* disulfide bond to construct DSPE-PEG-miRNA (Figure S1a). Then, the DSPE-PEG-miRNA was mixed with DSPE-PEG-Maleimide and fluorescent PFBT to induce NP formation through precipitation.[36,37] Finally, the miNPs were modified with the TAT peptide to facilitate NP uptake by the cardiovascular cells, which was grafted onto the maleimide group (Figure S1b).

TEM analysis revealed that miNPs are in a spherical shape, with an average size of ~110 nm and a narrow dispersity determined by a dynamic laser scattering instrument (Figure 1b,c). In comparison to NPs without miRNAs, the zeta potential of miNPs was lowered by ~15 mV, indicating successful surface presentation of miRNA (Figure 1d). To mimic the clinical application, which requires drug transportation and storage with prolonged shelf life, miNPs were frozen at −80 °C and thawed at room temperature for a total of 6 cycles. After each freeze−thaw cycle, the average size, size distribution, and zeta potential were quantified. As demonstrated in Figure 1e and f, there were negligible changes in miNP size and distribution in comparison to fresh miNPs throughout 6 cycles of freeze−thaw. The zeta potential became significantly lower from 22 to 20 mV after the first freeze−thaw, then stayed consistent throughout further cycles (Figure 1g). When the miNPs were encapsulated by ELP-HA hydrogel, more than 30% of miNPs were released after 5-day incubation with matrix metalloprotein 9 (MMP-9), which is expressed in ischemic myocardium. On the contrary, only 10% of miNPs were released from the hydrogel in the absence of MMP-9 (Figure 1h).

We hypothesized that our miRNA delivery system would provide efficient release of miRNA, triggered by the cleavage of disulfide bonds by intracellular glutathione (GSH), which exists in abundance in cardiac cells as an intermediate metabolite.[38] To test the feasibility of this strategy, the release of miRNA induced by GSH was first examined *in vitro*. To further confirm that the released miRNAs were intact, high-sensitivity microfluidic-based small RNA analysis was performed to detect their sizes. In Figure 1i, the released miRNA

DOI: 10.1021/acsnano.9b03343
ACS Nano 2019, 13, 9880−9894

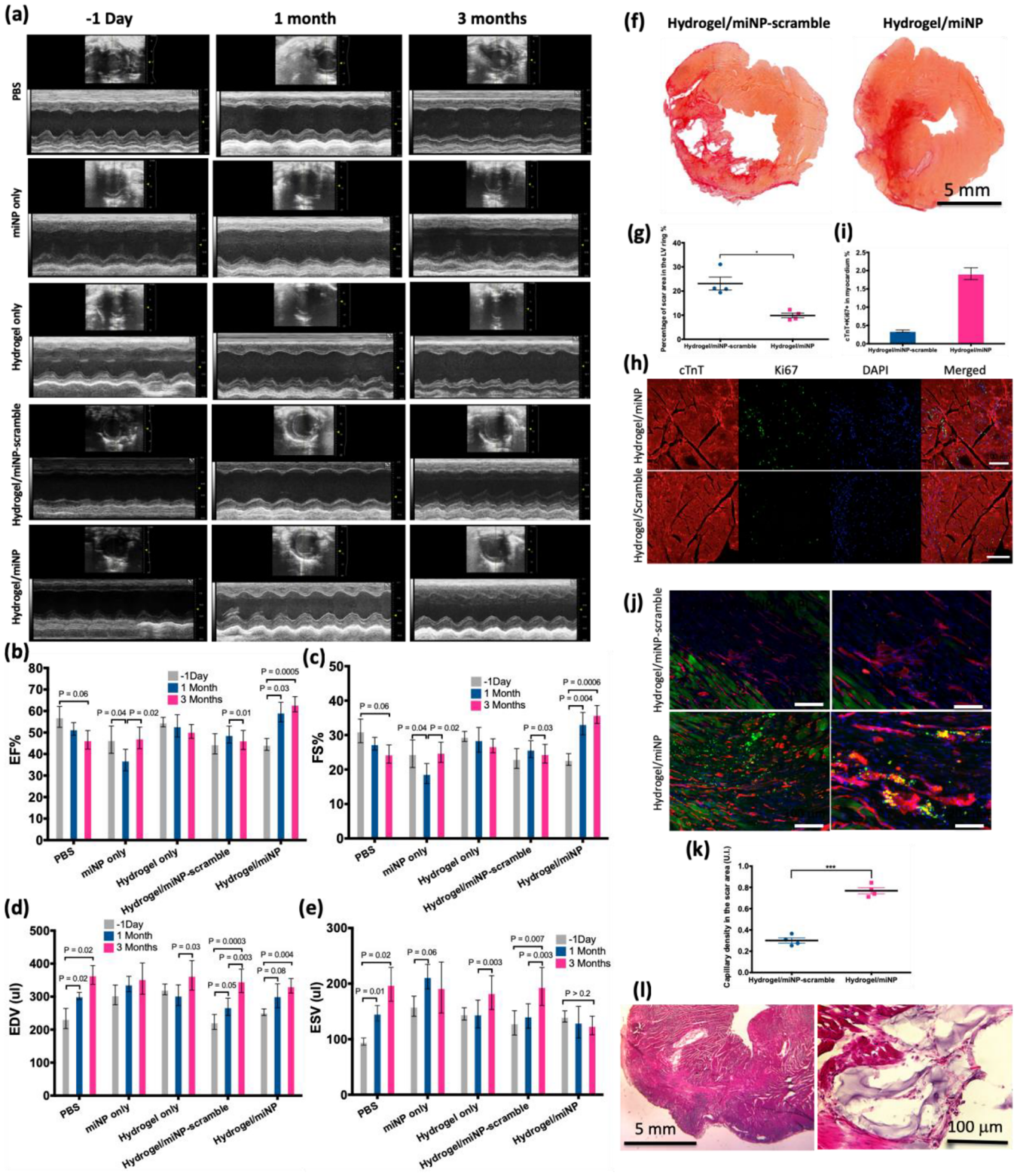

Figure 3. Cardiac function assessments in the rat ischemia/reperfusion model up to three months. The cardiac function of rats was evaluated by the cardiac echography within five groups: PBS, miNP, hydrogel, hydrogel/miNP-scramble, and hydrogel/miNP. (a) The representative corresponding b-mode and m-mode ultrasound images of a parasternal short-axis view of a rat heart at −1 day, 1 and 3 months in the PBS, miNP, hydrogel, hydrogel/miNP-scramble and hydrogel/miNP groups. (b) The improved EF in the hydrogel/miNP group, worsened EF in the PBS group and preserved EF in the miNP, hydrogel, and hydrogel/miNP-scramble groups. (c) The improved FS in the hydrogel/miNP group, worsened FS in the PBS group and preserved FS in the miNP, hydrogel, and hydrogel/miNP-scramble groups. (d) Dilated LV with increased EDV in all the groups. (e) Preserved ESV in the hydrogel/miNP group, significantly increased ESV in PBS, miNP, hydrogel, and hydrogel/miNP-scramble groups. (f) Images of fibrosis in the hydrogel/miNP and hydrogel/miNP-scramble groups evaluated by Picro Sirius Red staining. (g) Quantification of scar sizes in the hydrogel/miNP-scramble and hydrogel/miNP groups. (h) Confocal images of fluorescent immunostained Ki67 in green, cTnT in red and DAPI in blue of left ventricular tissue sections from the hydrogel/miNP and

DOI: 10.1021/acsnano.9b03343
ACS Nano 2019, 13, 9880−9894

Figure 3. continued

hydrogel/miNP-scramble groups at 1 month. (i) Quantification of double positive Ki67+ and cTnT+ CMs in (h) from the hydrogel/miNP and hydrogel/miNP-scramble groups at 1 month. $N = 4$. (j) The histological analysis of angiogenesis in myocardium within two groups: hydrogel/miNP-scramble and hydrogel/miNP, evaluated by the immunofluorescent imaging of capillary (red), miNPs (green), and nuclei (blue). (k) Over doubled capillary density of the infarction border zone in hydrogel/miNP group as compared to that in the hydrogel/miNP-scramble group. $N = 4$. *$p < 0.5$, **$p < 0.01$, ***$p < 0.001$. (l) Images of H&E stained left ventricular tissue section with injection of hydrogel/miNP at 1 month. A stable engraftment of hydrogel was observed within the myocardium, and no immune response was observed.

that was triggered either by GSH or DTT preserved its entire sequence with the same number of nucleotides in comparison to the freshly synthesized miRNA.

miNP Uptake within Human Cardiovascular Cells. To validate the miNP design and synthesis for better transfection efficiency, we chose the hESC derived CMs and ECs as an *in vitro* human model, which is well-developed with extended applications for studying cardiovascular diseases in our lab.[39,40] First, validation of hESC differentiation down CM and EC lineages were confirmed by immunostaining (Figure S2). The results of miNP uptake 24 h after transfection are shown in Figure 2. The average uptake in hESC-CMs was over 60% when the initial feeding concentration was lower than 100 nM (Figure 2b). The NP uptake in hESC-CMs increased along with increasing feeding concentrations of NPs, reaching a peak at 100 nM, then starting to decrease at 200 nM as shown in Figure 2b. The uptake of miNPs in hESC-CMs under hypoxic condition was significantly higher than that under normoxia at the miRNA concentration of 100 nM (Figure 2c). A large amount of internalized miNPs was distributed in the cytoplasm around nuclei of hESC-CMs as shown in the confocal images (Figure 2d). With increasing loading concentration of miRNA, the uptake percentage by hESC-ECs was gradually decreased, and the optimal concentration for hESC-ECs was 50 nM based on a comprehensive consideration of percentage and absolute amount of uptake (Figure 2e). Additionally, there was less miNP uptake by hESC-ECs in the hypoxic condition compared to the normoxic condition (Figure 2f).

miNP Cytotoxicity in Human Cardiovascular Cells. A primary consideration when designing gene therapy delivery strategies is cytotoxicity; therefore, the cytotoxicity of miNPs on the major cell types in myocardium, CMs, ECs, and cardiac fibroblasts (CFs), was assessed. In Figure 2g, the enhanced viability of hESC-CMs was demonstrated in the miNP group with increased concentrations of miRNA with the peak concentration at 100 nM; by comparison, a consistent number of cells was observed in the lipofectamine RNAiMAX (lipo) group with miRNA loading concentrations ranging from 12.5 to 100 nM (Figure 2g). A further increase of miNP concentration from 100 to 200 nM in cell culture caused a slight drop of hESC-CM viability, whereas the lipo group experienced a worsen cytotoxicity below the starting amount at the same concentration. The viability of hESC-ECs had a similar trend upon incubation with miNPs, while hCFs showed maintained viability with increasing concentrations of miNPs (Figure 2h,i). In all three groups, lipofectamine RNAiMAX exhibited significantly higher cytotoxicity than miNPs when the miRNA concentration was above 25 nM.

Cardiac Function Improvement with miNP Delivery by Injectable Hydrogel. Next, the *in vivo* miNP delivery system was applied in a rat MI model. Four days post-MI, one dose of miNP along with injectable hydrogel at 3 spots was administered at the border zone of MI in beating left ventricle (LV), as illustrated in Figure S3. The dose of miRNA was determined by the comprehensive evaluation of miNP's transfection efficiency and biocompatibility as obtained above. NPs carrying scramble miRNAs (miNP-scramble) were also prepared and used in a control group. In animal experiments, 5 groups of rats were treated by PBS, miNP, hydrogel, hydrogel/miNP-scramble, and hydrogel/miNP, respectively. Due to the shear-thinning and rapid self-healing properties of the hydrogel (Figure S4), a smooth and fast injection was conducted, with high retention in the myocardium. This engraftment of hydrogel and host myocardium was found in the histology analysis after 4 weeks. After 3 months, no hydrogel was detected in the myocardium and release of miNPs was profound (Figure S5). The cardiac function was assessed by echocardiography at day −1, 1 month and 3 months, as shown in Figure 3a. The ejection fraction (EF) of rats in hydrogel/miNP group increased from day −1 to 3 months (Figure 3b). The absolute increase of EF at 1 and 3 months using the EF value at the day −1 as baseline is 15% and 19%, respectively. On the contrary, the EF preserved in hydrogel and hydrogel/miNP-scramble treated groups. In addition, the PBS group demonstrated a physiopathologically worsened cardiac function with gradually decreased EF, while a fluctuated EF was noticed in the miNP group without hydrogel. Moreover, the fraction shortening (FS) showed a similar trend of change to the EF of these five groups (Figure 3c). The left ventricle end-diastolic volumes (EDV) increased gradually in all the five groups (Figure 3d). Noteworthy is that the left ventricle end-systolic volume (ESV) was preserved in hydrogel/miNP group while it significantly increased in the other four control groups from −1 day to 3 months (Figure 3e).

Ex vivo analyses were then carried out to further validate the *in vivo* results. First, the scar size in left ventricle determined by Picro Sirius Red staining was 20% and 10% in hydrogel/miNP-scramble and hydrogel/miNP group, respectively. (Figure 3f,g). The *in vivo* CM proliferation in the border zone was also confirmed through immunofluorescence staining with double expression of Ki67 in red and cTnT in green (Figure 3h). Statistical analysis of 4 samples in each group revealed that more than 2% of CMs in the tissue sections of hydrogel/miNP group were in cell cycle while only less than 0.2% of CMs from hydrogel/miNP-scramble group were in cell cycle (Figure 3i). The angiogenesis induced by released miNPs from hydrogel was also observed in the adjacent area (Figure 3j), where abundant miNPs were released and partially taken up by the capillaries. Quantitative analysis revealed that the capillary density in the scar area in the hydrogel/miNP group was more than twice that of the hydrogel/miNP-scramble group (Figure 3k). Moreover, the injected hydrogel demonstrated functional engraftment within the myocardium at 1 month post-treatment, and no obvious immune response was observed from H&E staining results (Figure 3l).

Function of miNP in the Human Cardiovascular Cells under Hypoxic Condition. To unveil the mechanism of

DOI: 10.1021/acsnano.9b03343
ACS Nano 2019, 13, 9880−9894

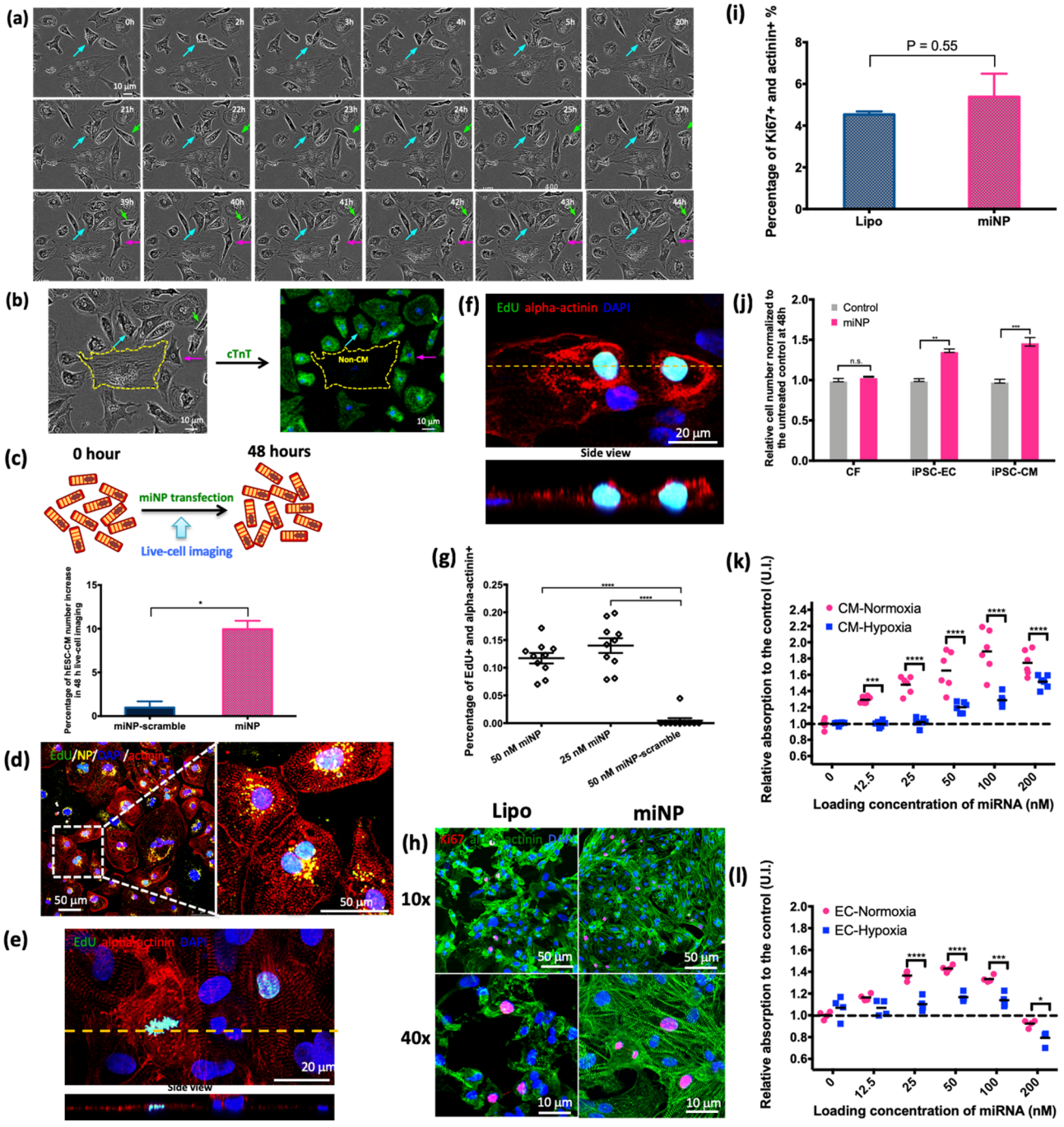

Figure 4. Enhanced proliferation of hESC derived cardiovascular cells. (a) The phase-contrast live-cell imaging by IncuCyte over 48 h in corresponding to the Supplementary Video S1, arrows indicate the proliferating cells. Scale bar: 10 μm. (b) Coordination of the end-point (at 48 h) live-cell phase-contrast and immunostained fluorescent images of troponin T (green). The yellow dash line contoured the non-CM. Scale bars: 10 μm. (c) Percentage of hESC-CM number increase in 48 h using live-cell imaging by IncuCyte along with a cartoon illustration. (d) Confocal images of hESC-CMs transfected with PFBT miNPs (yellow) and stained by EdU (green), alpha-actinin antibody (red), and DAPI (blue), indicating the miNP uptake and CM proliferation. The overlap of EdU (green) and DAPI (blue) signals appears in cyan color. Scale bars: 50 μm. (e) and (f) Different cell cycle stages of hESC-CMs treated with PLGA miNPs, followed by staining with EdU (green), alpha-actinin (red), and DAPI (blue). Scale bars: 20 μm. (g) The ratios of double positive EdU and alpha-actinin stained hESC-CMs treated with miNP or miNP-scramble at miRNA concentrations of 25 and 50 nM, respectively. N = 10. (h) Confocal images of Ki67 (red), alpha-actinin (green) and nuclei (DAPI, blue) in hESC-CMs treated with miNP or lipofectamine RNAiMAX/miRNA. 40×. (i) Ratios of double positive hESC-CMs of Ki67 and alpha-actinin treated with miNP, or lipofectamine RNAiMAX/miRNA in normalization to the control group. p = 0.55 of miNP *vs* lipo. (j) Relative cell numbers of hESC-CMs, hESC-ECs and hCFs at 48 h to the cell numbers at 0 h after miNP treatment, N = 4. (k) Hypoxic condition relatively decreases the cell proliferation of hESC-CMs at varied miRNA loading concentrations as compared to the normoxic condition. (l) Hypoxic condition relatively decreases the cell proliferation of hESC-ECs at varied miRNA loading concentrations as compared to the normoxic condition. n.s.: no significance, *p < 0.05, **p < 0.01, ***p < 0.001, ****p < 0.0001, N = 4−6 in each group.

DOI: 10.1021/acsnano.9b03343
ACS Nano 2019, 13, 9880−9894

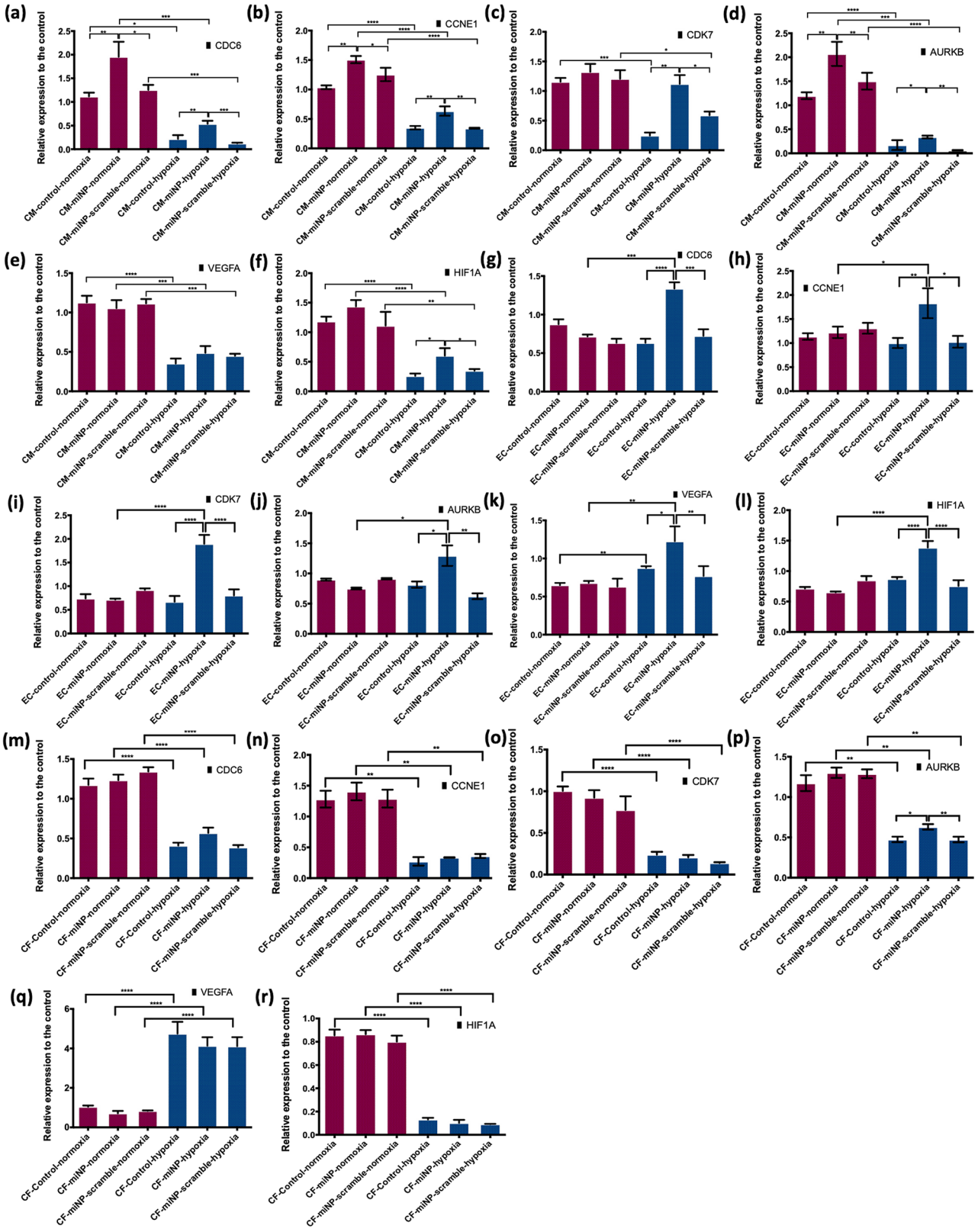

Figure 5. Relative gene expressions in human cardiovascular cells treated with miNP or miNP-scramble in normoxic or hypoxic condition. CDC6, CCNE1, CDK7, AURKB, VEGFA, and HIF1A expression in hESC-CMs (a–f), hESC-ECs (g–l), and hCFs (m–r). $*p < 0.05$, $**p < 0.01$, $***p < 0.001$, $****p < 0.0001$.

miNPs in promoting myocardium recovery as found in the *in vivo* rat MI model, the functions of miRNA-199a-3p were further explored and investigated in the cellular model using hESC-CMs, hESC-ECs, and hCFs. First, the results of the *in situ* live-cell imaging is demonstrated in Figure 4a. A corresponding *in situ* time-lapse video (Video S1) was recorded to corroborate the cell proliferation in real time, and immunostaining of cardiac troponin T (cTnT) further

DOI: 10.1021/acsnano.9b03343
ACS Nano 2019, 13, 9880–9894

confirmed that the divided cells were CMs based on simultaneous phase contrast images in the video (Figure 4b). After 48 h transfection, around 10% increase of cell number of hESC-CMs in the miNP treated group and less than 2% cell number increase of hESC-CMs in the miNP-scramble group were demonstrated in Figure 4c. Then, EdU was successfully integrated into the nuclei to distinguish the dividing or daughter hESC-CMs with internalized miNPs around the nuclei as shown in Figure 4d. The double staining of alpha-actinin and EdU confirmed that the cells in cell cycle re-entry were hESC-CMs (Figure 4e,f). After analyzing over 1000 hESC-CMs, accumulatively 10% cells were found to be double positive for alpha-actinin and EdU when transfected with miNPs at low (25 nM) and high (50 nM) miRNA concentrations (Figure 4g). In the meanwhile, the cell cycle marker Ki67 was also examined in hESC-CMs after a 48 h transfection with either miNP or lipo. The double-positive cells expressing Ki67 and cardiac alpha-actinin were frequently observed as shown in Figure 4h. Quantitative analysis of the images revealed that the ratios of double-positive cells with Ki67 and alpha-actinin in both miNP and lipo groups were over 5% (Figure 4i). However, the hESC-CMs preserved striated sarcomere in the miNP group, whereas the lipo group had disassembled sarcomere due to the toxic effect of lipo (Figure 4h). The proliferation assay was also carried out using hESC-ECs and hCFs. As shown in Figure 4j, hESC-ECs and hESC-CMs had significantly increased cell numbers at 48 h, but the number of hCFs did not show significant difference before and after treatment (Figure 4j). To further examine the proliferative effect in the hypoxic condition of hESC-ECs and -CMs, the cell proliferation was still activated in the higher loading concentration of miRNA (>25 or 50 nM in hESC-EC and -CM, respectively) although the proliferation in both of hESC-CMs and -ECs were relatively suppressed at the low loading concentration of miRNA (Figure 4k,l).

Moreover, the transcriptional expressions that can be affected by the cell cycle, angiogenesis, and hypoxic responses were evaluated in hESC-CMs, hESC-ECs, and hCFs using real-time quantitative PCR (RT-qPCR) as shown in Figure 5. In the normoxic condition, CDC6, CCNE1, and AURKB in hESC-CMs had significantly higher expression in treated groups in comparison to the control groups (Figure 5a−d). Under hypoxic condition, the four cell cycle related genes of CDC6, CCNE1, CDK7, and AURKB tended to be suppressed in all three types of cardiovascular cells. However, these genes were relatively up-regulated in the hESC-CMs and -ECs upon treatment with miNPs (Figure 5a−d,g−j), indicating that the cells tended more to be in the G1/S and S/M phases even under the hypoxic condition. For hCFs, there was no significant difference before and after miNP treatment either in normoxia or hypoxia (Figure 5m−p). An up-regulation of VEGFA expression was observed in both of the hypoxia treated hESC-ECs and hCFs (Figure 5k,q), whereas its expression was suppressed in the hESC-CMs (Figure 5e). With the treatment of miNPs, a boost of VEGFA expression was detected in the hESC-ECs (Figure 5k), while there was no response regarding the VEGFA expression in both hESC-CMs (Figure 5e) and hCFs (Figure 5q). Additionally, the suppressions of HIF1A expression due to the hypoxic conditioning were found in the hESC-CMs (Figure 5f) and hCFs groups (Figure 5r), and both hESC-CMs and hESC-ECs expressed more HIF1A with coculture of miNPs than those in the scramble group under the hypoxic condition (Figure 5f,l).

To further validate the effect of miNP on vascular function and angiogenesis, we performed the tube formation assay with hESC-ECs at normoxia and hypoxia. More tubes were formed in the miNP treated group at both normoxic and hypoxic conditions (Figure S6a). The statistic analysis using ImageJ Angiogenesis Analyzer reveals that more nodes, junctions, and branches were formed in the miNP group under normoxia and hypoxia (Figure S6b). Meanwhile, we also conducted the fibrosis contraction assay with hCFs. After 24 h incubation, the mixture hCFs and type I collagen at normoxia or hypoxia showed contracted construction in all three groups. However, no significant difference among the control, miNP-scramble, and miNP groups was observed in either normoxia or hypoxia (Figure S6c,d).

DISCUSSION

By interacting and silencing mRNAs (mRNAs), miRNAs act as small noncoding RNAs and play a significant role in the transcriptional regulation of genes in cardiovascular development, pathology, and regeneration.[11] In the past decade, several miRNAs have been implicated in cardiac regeneration, particularly by restoring the functions of damaged myocardium. For instance, miR-195 and miR-29a act through cell cycle of CMs by targeting cyclinD1.[12] The increased expression of miR302−367 cluster was found to lead to profound proliferation of CMs in mice *via* the Hippo pathway;[41] Giacca and colleagues conducted high-throughput miRNA screenings and found that miR-199a-3p and miR-590-5p were capable of triggering the cell-cycle re-entry of rat and mouse adult/neonatal CMs through targeting the CLIC5 and HOMER1.[16] These discoveries of miRNAs' significant role in the proliferation of CMs raise further possibilities for future clinical therapies to restore the function of the damaged heart and eventually regenerate heart tissue.

To successfully implement potential miRNA-based therapies in the future, a safer and more efficient *in vivo* delivery method is urgently needed. Previously, AAV and commercialized lipocomplexes were applied to encapsulate miRNAs for *in vivo* delivery, improving cardiac function and reducing the scar size of infarcted myocardium in rat and mouse models.[15,16] However, although lipocomplex does not have the same safety concerns or tumorigenic risks as AAV,[20,21,42] its high cytotoxicity and *in vivo* instability are obstacles for further biomedical translation.[43] Therefore, a better clinical translational *in vivo* delivery and transfection approach as described in this study is needed to tackle those problems.

In this study, miNPs were rationally designed and synthesized for *in vivo* delivery of miRNAs in the long term. The conjugated polymer (PFBT) with stable fluorescence and good biocompatibility can ensure accurate tracking of the localization of miNPs.[44] DSPE-PEG was chosen as the encapsulation matrix because the conjugation between small interfering RNA and poly(ethylene glycol)-lipid was found to improve the stability of RNA segments against enzymatic degradation[45] and the functional group of DSPE-PEG can facilitate functionalization with TAT peptide to transfect miRNA in cells with high efficiency. The obtained miNPs showed a narrow distribution with excellent quality control and ideal size of ∼110 nm for optimal cellular uptake.[46] For better application in the clinic and to address common concerns of using NP for drug delivery,[47] the stability of miNPs was tested by cycles of freezing and thawing. We found that the miNPs successfully maintained its size, distribution, and surface charge

DOI: 10.1021/acsnano.9b03343
ACS Nano 2019, 13, 9880−9894

for up to 6 cycles (>6 cycles was not tested here), demonstrating its stability for shipment and flexibility of use. Moreover, we found that the release of miRNA from miNPs was triggered either by GSH or DTT at physiological temperature, and its nucleotide length was kept intact with validated therapeutic functions. We also found no differences between freshly synthesized miNPs and miNPs stored for over 6 months at −80 °C in terms of size, distribution, surface charge, or miRNA integrity, suggesting that the miNP has a very long shelf life. Overall, our results indicate that the quality of miNP can meet the comprehensive requirements for use in miRNA encapsulation and further medical applications.

In the past decade, *in vitro* human cell/tissue models for biosystems such as the cardiovascular system, hepatic system, and neuronal system have been established *via* advances in hiPSC technique and proper differentiation protocols.[39,40,48−52] As expected, the extremely low cytotoxicity of miNPs in comparison to the lipo at 48 h was confirmed by the cell viability assay. Additionally, the hESC-CM dysfunction caused by lipo was reflected in the disarrayed cardiac sarcomere, which is essential for cardiac contraction and mechanical couplings.[53,54] Specifically, in comparison to the commercial lipocomplex,[15] miNPs had very low toxicity to the hESC-CM/-EC and hCFs even at high miRNA loading concentrations (100 nM for hESC-CMs, 50 nM for hESC-ECs), indicating the miNPs could act as a high capacity carrier for miRNAs with a negligible risk of damage to human cardiovascular cells. Overall, our results also demonstrate a promising solution for the efficient delivery of high quantities of therapeutic molecules to target spots, which is still challenging in the drug delivery field.[23,55]

One significant aspect of the miNP is that it is designed to be taken up efficiently, especially by cardiovascular cells, which otherwise are difficult to be transfected efficiently with nonviral methods.[56] To achieve this goal, we integrated an additional cell-penetrating peptide (CPP) on the outer layer of miNP's shell to facilitate the transfection efficiency of miRNA in human cardiovascular cells. With the assistance of TAT as a CPP, which has shown potential in preclinical and clinical applications in the past decade,[57,58] more than 60% of miNPs were internalized into the human cardiovascular cells (hESC-CMs, hESC-ECs, and hCFs) with extremely low leakage, ensuring the maximized release of miRNA inside the cytoplasm. The high efficiency of transfection was also verified in the *in vitro* hypoxic condition, which recapitulated the ischemic microenvironment of the myocardial infarction. We found there was only less than 10% variation in miNP uptake for the hESC-CMs and hESC-ECs from the hypoxic treatment, suggesting our miNP system would also be applicable in cardiovascular ischemic situations. The excellent performance of miNP-assisted miRNA transfection in the human cardiovascular system in both normoxic and hypoxic conditions makes it a promising approach for miRNA delivery to the cardiovascular cells in the infarcted area.

After *in vitro* evaluation of miNPs, the *in vivo* studies were carried out to further investigate the feasibility and performance of miNP *in vivo* delivery for cardiac function restoration in a rat model. The ischemia/reperfusion procedure creates an ideal MI model in rats.[59] Without proper treatment to postpone the deterioration of the infarcted cardiac muscles, the myocardium will undergo remodeling in terms of dilated ventricle and increased wall stress, resulting in a gradual drop of pumped blood volume as the outcome in our PBS group.[60] The miNPs were efficiently delivered along with a shear-thinning hydrogel *via* direct injection into the beating heart without leakage as proven explicitly in our previous study.[28] The ELP based hydrogel has shown capability of releasing the encapsulated reagent, such as growth factors and nanoparticles, especially in injured tissues.[34] While the EF% and FS% were preserved in both of the hydrogel and hydrogel/miNP-scramble groups, the hydrogel/miNP administration successfully improved EF% and FS% by ∼19% in comparison to the EF% and FS% at day −1, matching the results of AAV delivery[16] and exceeding the outcome of the commercial lipo delivery.[15] The preserved ESV in the hydrogel/miNP group over 3 months in comparison to the groups of hydrogel only, miNP only, and hydrogel/miNP-scramble indicate that the contraction of the left ventricle was significantly maintained due to the miRNA interference caused heart muscle regeneration,[15,16] which also reduced scar size by half. The *in vivo* CM proliferation was also promoted by the hydrogel/miNP with a higher percentage of proliferative CM in the infarct zone, confirmed by immunofluorescence staining results. Furthermore, capillary growth was also enhanced in the border zone with miNP uptake, suggesting that the activation of angiogenesis was involved in restoring cardiac function as well. The revascularized myocardium can actively improve the cardiac function, which is considered as a key factor of successful therapeutic intervention.[61] Importantly, the cardiac function continued to improve in a long-term (3 months) with just one dose of miNP injection, demonstrating the potential of our miNP delivery system in reducing the number of risky invasive clinical interventions currently required for lifetime treatment.

To further understand the molecular mechanism of miNP treatment on the human cardiovascular system, we established an *in vitro* model using the hESC-derived cardiovascular cells, which have shown multiple advantages in drug evaluation and discovery for humans.[48,51,62−64] In our study, we confirmed the function of miRNA-199a-3p with the cell cycle re-entry of hESC-CMs, demonstrating similar rate of cell proliferation in miNP treated group as previously reported on the rat/mouse neonatal CMs.[16] The up-regulation of cell cycle genes indicated that the miNPs successfully activated hESC-CMs to G1/S and S/M phases by initiating DNA replication and mitosis, confirming that miNP-treated CMs can undergo proliferation for cardiac function restoration.[65,66] Additionally, the miNPs also boosted proliferation of hESC-ECs under ischemic condition, which could be another significant regenerative effect in restoring the function of infarcted myocardium as found in the rat model.[17,67,68] The *in vitro* tube formation assay has been commonly used in the vascular function and angiogenesis evaluation.[39,69] The enhanced formation of tube nodes, junctions and branches determined in this assay further supported the theory that miNPs can improve vascular function and angiogenesis. Overall, the result of *in vitro* modeling with hESC-ECs can explain the increased capillary density in the infarct border zone in the hydrogel/miNP-treated rat myocardium. On the other hand, miNPs did not show effect on promoting the cell cycle gene activation and cell number increase of hCFs, easing the concern that excessive proliferation of fibroblasts might induce extended fibrosis under miNP treatment.[19] Moreover, *in vitro* fibrosis contraction assay validated that the miNPs did not functionally promote cardiac fibrosis. We believe that after miNP treatment, the promoted proliferation of CMs and ECs

DOI: 10.1021/acsnano.9b03343
ACS Nano 2019, 13, 9880−9894

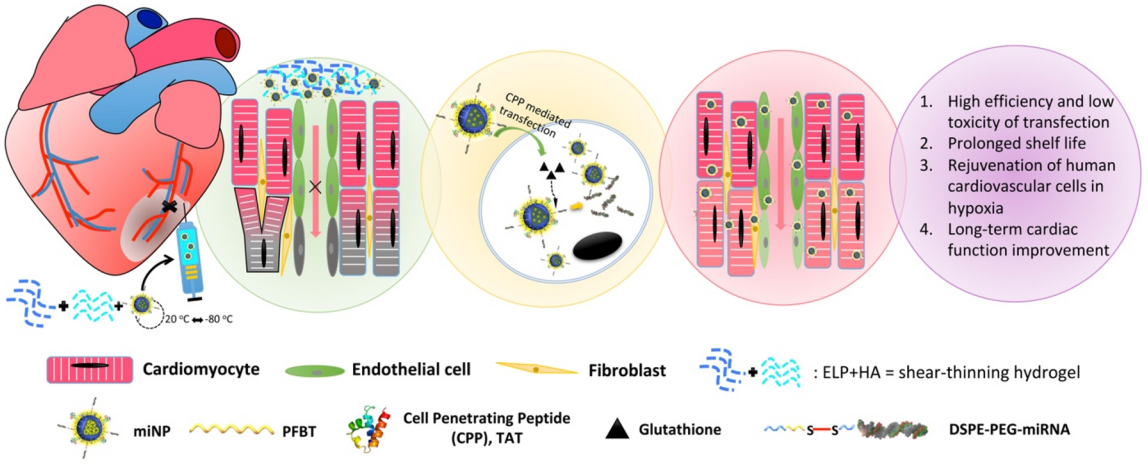

Figure 6. Schematic summary of miNP *in vivo* delivery system for restoring the infarcted myocardium. miRNA was successfully encapsulated and further delivered *via* the comprehensively designed shear-thinning hydrogel/miNP system into the border zone of myocardial infarction, and the released miNPs were efficiently uptaken by the cardiomyocytes and endothelial cells with the assistance of cell penetrating peptide. Since the miNPs entered into the cytoplasma, the miRNAs were readily released and then interacted with mRNAs to regulate the cellular function of cardiovascular cells to further restore the function of infarcted myocardium through activating the cell cycle re-entry, angiogenesis, and antiapoptosis of cardiomyocytes and endothelial cells.

without triggering the proliferation of CFs contributed to the outcome of reduced scar size in the infarcted myocardium.

Moreover, we recapitulated the ischemic microenvironment in the infarcted myocardium by introducing the hypoxic treatment to each cell type under varying loading concentrations of miNPs. It is known that low oxygen supply can inhibit the proliferation of cardiovascular cells, causing cell death and MI.[70−72] Although the proliferation of hESC-CMs and -ECs was slightly suppressed under hypoxia and remained unchanged upon treatment with miNPs at low concentrations, the proliferation of these cells was promptly activated when more miNPs (in the range of working concentrations) were internalized into the cells, suggesting the therapeutic activity of miNPs can be profound in an ischemic environment. This finding is consistent with the results obtained at the transcriptional level with RT-qPCR studies. It seems that hESC-ECs were more sensitive to hypoxia with 1.5 to 3 times higher up-regulation of CDC6, CCNE1, AURKB, and CDK7 after incubation with miNPs. Also, miNP treatment also led to up-regulation of HIF1A in both hESC-CMs and -ECs, and up-regulation of VEGFA in the hESC-ECs.[72,73] HIF-1 (HIF1A) is the master regulator of oxygen utilization and delivery in the heart, and promoting the HIF1A expression can benefit the cardiovascular system.[72] More importantly, HIF-1 is found to be required for the proliferation of fetal cardiomyocytes in the ischemic condition by regulating the cardiac metabolism and cell cycle,[74] which may also be the mechanism for the enhanced miNP-induced proliferation of hESC-CMs in the hypoxic condition. Because the up-regulation of HIF-1/VEGF pathway and better tube formation in the miNP-treated group promoted the vascular response by significantly increasing the capillary density in border zone, it may represent a vital target for triggering cardioprotection in the failing heart.[72] In the future, it is critical to understand whether the newly formed vasculature is functional in blood circulation system, and the *in vivo* arteriogenesis study will be carried out to unveil it. Overall, our results indicate that miNP may work by activating the cell cycle re-entry of CMs and ECs, endothelial functions, and by using HIF-1/VEGF pathway to improve the cardiac function of post-MI effectively.[70,71]

CONCLUSION

We have successfully designed a robust *in vivo* localized miRNA delivery system using polymeric nanoparticles (miNPs) and injectable hydrogel with translational potential for post-MI treatments, as illustrated in Figure 6. The prolonged shelf life and excellent tolerance to freezing/thawing cycles of miNPs were confirmed with stable characteristics of nanoparticles and intact released miRNAs in the physiological conditions, while the extremely high uptake efficiency and good retention of miNPs were validated by hESC-CMs and hESC-ECs in both normoxia and hypoxia. Localized miRNA delivery into the infarcted myocardium through hydrogel/miNP composites significantly improved cardiac function in the 3-month ischemia/reperfusion rat model by restoring the contractility of damaged myocardium, with reduced scar size and increased capillary density in the border zone. Moreover, results from the *in vitro* modeling with hESC-derived cardiovascular cells showed that miNP triggered the activation of cell cycle re-entry, which was mainly valid for hESC-CMs and hESC-ECs, but not for hCFs, leading to the smaller scar size and no effect on fibrosis. Mechanism investigation revealed that our approach also had additional beneficial effects by restoring cardiac function through improving vascular function and angiogenesis, confirmed by the up-regulated expression of VEGFA and HIF1A in hESC-CMs and hESC-ECs and better tube formation in *in vitro* assays.

Overall, our *in vivo* miRNA delivery system has significant potential for realizing future miRNA therapy in treating MI, given its extremely high biocompatibility and transfection efficiency as demonstrated in both of *in vitro* and *in vivo* models exposed to ischemic conditions. A single dose of hydrogel/miNP injection was able to significantly and continuously restore the infarcted myocardium, enhancing cardiac function with regenerated and neovascularized myocardium for up to three months. Finally, using the latest hESC and proper cardiovascular cell differentiation techniques, we were able to validate the mechanism of miRNA-induced CM and EC proliferation and hypoxic responses as shown by our *in vivo* results. In summary, we have successfully

DOI: 10.1021/acsnano.9b03343
ACS Nano 2019, 13, 9880−9894

established a clinical translational delivery system for miRNA-based therapy on restoring infarcted myocardium with extraordinary advantages in high biocompatibility, efficient transfection, and prolonged shelf life.

METHODS

Materials for Nanoparticle Synthesis. Reduced glutathione (GSH), dithiothreitol (DTT), poly(9,9-dioctylfluorene-*alt*-benzothiadiazole) (PFBT), poly(D,L-lactide-*co*-glycolide), dimethyl sulfoxide (DMSO), and tetrahydrofuran (THF) were purchased from Sigma-Aldrich. DSPE-PEG-Maleimide (M_w = 5000) and DSPE-PEG-Amine (M_w = 3400) are commercial products from Laysan Bio, Inc. Thiol-modified cell penetrating peptide (CCP), RKKRRQRRRC, was customized by GenicBio, China. 3-(2-Pyridyldithio)propionate (SPDP) linker was purchased from Thermo Fisher Scientific. miR-199a-3p mimic: ACAGUAGUCUGCACAUUGGUUA, and miR-199a-3p scramble mimic: GAAACGCUUCAUGUACGUAGUU were designed by InvivoGen siRNA design wizard v3.1 and synthesized at the Stanford Protein and Nucleic Acid Facility (PAN).

Conjugation of miRNA to DSPE-PEG-Amine. DSPE-PEG-miR-199a-3p was synthesized by conjugating DSPE-PEG-Amine and thiol-modified miRNA at 5′ end, using SPDP as a linker. First, DSPE-PEG-Amine (10 μmol) and SPDP (1 μmol) were mixed in 5 mL of DEPC-treated 1× PBS buffer (pH 7.4) for 2 h at room temperature under stirring. To eliminate excess SPDP, the mixture was then washed with an Amicon Ultra-4 centrifugal filter unit with ultracel-10 membrane (MWCO 3 kDa) twice using DEPC-treated DI water. The concentrated solution was further diluted in 5 mL of DEPC-treated 1× PBS buffer (pH 7.4) and miRNA (0.1 μmol) was added for overnight reaction at 4 °C. The reaction mixture was purified using an Amicon Ultra-4 centrifugal filter unit with ultracel-10 membrane (MWCO 30 kDa and 10 kDa) 3 times with DEPC-treated 1× PBS buffer and then 5 times with DI water. The concentrated product was dialyzed against DEPC-treated DI water for 2 days using a dialysis tube (MWCO 12−14 kDa), followed by freeze-drying to obtain powder for further use. DSPE-PEG-miRNA-Cy5.5 was synthesized following the same procedures for quantification study later.

Synthesis of TAT-Conjugated miNPs. The TAT-conjugated miRNA-NPs (miNPs) were synthesized through a modified nanoprecipitation method. PFBT (2 mg), DSPE-PEG-miRNA (4 mg), and DSPE-PEG-Maleimide (2 mg) were weighed and dissolved in 1 mL of THF. The THF solution was quickly injected into DEPC-treated DI water, followed by continuous sonication using a probe sonicator for 90 s. The suspension was washed 5 times with water using an Amicon Ultra-4 centrifugal filter unit (MWCO 10 kDa) to eliminate THF. The suspension was then filtered through 0.2 μm syringe filters and diluted in 5 mL of DEPC-treated 1× PBS buffer (pH 7.4), followed by addition of TAT peptide solution (4 μmol). Reaction was carried out under stirring at 4 °C overnight, and the mixture was washed with 1× PBS and water to obtain concentrated TAT-PFBT-miRNA NPs (miNPs). To synthesize TAT-conjugated NPs without miRNA (NPs), DSPE-PEG-Maleimide was solely used and the same procedures were followed.

Characterization of miNPs. The average particle size and zeta potential of miNPs were determined by a Zetasizer Nano ZS equipment at room temperature. The morphology of miNPs was studied by a FEI Tecnai G2 F20 X-TWIN Transmission Electron Microscope.

miRNA Release. Both reduced GSH and DTT were used to cleave the disulfide bond to release miRNA from miNPs. miNPs (0.5 mL) was mixed with 5 mL of GSH (10 mM) and DTT (100 mM) in 1× PBS buffer (pH = 7.4) separately. Meanwhile, 0.5 mg of DSPE-PEG-miRNA was also mixed with 1 mL of GSH in 1× PBS buffer (pH = 7.4) separately. After incubation for 24 h at 37 °C, the mixtures were concentrated using Amicon Ultra-4 centrifugal filter units with ultracel-10 membrane (MWCO 10 kDa). The cleaved miRNA in concentrated samples were analyzed through Agilent Bioanalyzer QC with a standard ladder from 4 to 150 nucleotides.

Estimation of miNP Concentration and miRNA Concentration. First, the average volume of each miNP was estimated based on the average size of miNPs in water (~104 nm). As the nanoparticle suspension in water was stable, the density of nanoparticles should be close to that of water. By assuming the density of miNPs to be ~1 g/cm^3, the concentration of miNPs in stock suspension was calculated from the following equations:

The number of miNPs in stock solution:

$$\frac{\text{total volume of miNPs}}{\text{average volume of each miNP}} = \frac{\frac{6\times10^{-3}\ \text{g}}{1\ \text{g/mL}}}{\frac{4}{3}\pi\times(52\times10^{-7})^3\ \text{mL}} = 1.02\times10^{13}$$

The concentration of miNPs in 1 mL of stock solution:

$$[\text{miNP}]\frac{\frac{1.02\times10^{13}}{6.02\times10^{23}}\ \text{mol}}{1\ \text{mL}} = 17\ \text{nM}$$

The concentration of miRNA in final product was estimated using TAT-PLGA-miRNA-Cy5.5. PLGA was used as the core instead of PFBT to obtain TAT-PLGA-miRNA-Cy5.5 NPs following the same procedures, avoiding interference from absorbance and fluorescence of PFBT during quantification of Cy5.5. The maximum of UV−vis absorbance of Cy5.5 at 690 nm in diluted NP solution was measured. Through a calibration curve, the concentration of miRNA-Cy5.5 was calculated to be 4 μM in stock solution. The number of miRNAs immobilized on each nanoparticle was then calculated as following:

$$\text{miRNA:miNP} = \frac{4\ \mu\text{M}}{17\ \text{nM}} = 235{:}1$$

***In Vitro* Uptake and Cytotoxicity of miNPs in Human Cardiovascular Cells.** The human embryonic stem cell-derived cardiomyocytes (hESC-CMs) and human embryonic stem cell-derived endothelial cells (hESC-ECs) were differentiated from H7 hESCs according to our previous publications.[39,48] hESC-CMs were over 95% pure and double-positive of cardiac troponin T and alpha-actinin by flow cytometer after two rounds of glucose starvation, and were used at day 45 after differentiation. The cell maintenance medium of hESC-CMs was RPMI with B27 supplemented with insulin and 4% fetal bovine serum (FBS). The hESC-ECs were over 90% pure after magnetic-activated cell sorting through CD144 selection, and the passage of hESC-ECs used in this study was 1 to 3, and the hESC-ECs were maintained in Lonza EGM-2 BulletKit containing 2% serum. Human primary cardiac fibroblasts (hCFs) were purchased from Lonza and maintained in DMEM with 5% FBS. We used the same maintenance medium for the following miNP transfection experiments.

The *in vitro* uptake and cytotoxicity of miNPs were quantified using hESC-CMs, hESC-ECs, and hCFs. First, a 96-well plate seeded with 5000 cells per well was prepared. After 24 h incubation with the miNPs at varying loading concentrations of miRNA ranging from 0, 12.5, 25, 50, 100, and 200 nM, the 100 μL supernatant and the 100 μL rinsing medium (×2) of each well were collected to obtain the percentage of uptake relative to the loading concentrations. N = 6 in each loading concentration. To recapitulate the microenvironment of ischemic myocardium, the hypoxic condition was introduced in the entire process of miNP uptake and release. In brief, the 96-well plate with cells after the addition of miNPs was kept in the BD GasPak EZ pouch systems (Becton Dickinson) in the cell culture incubator, and the miNP uptake was measured accordingly as above.

At equal loading concentrations in the 96-well plate, the cytotoxicity of miRNAs to hESC-CM, hESC-ECs, and hCFs was examined by the CellTiter-Glo luminescent cell viability assay 2.0 (Promega). In brief, following the user's manual, 100 μL CellTiter-Glo reagent was added and mixed with 100 μL culture medium in each well, which was preseeded cells for 48 h; after 5 min

DOI: 10.1021/acsnano.9b03343
ACS Nano 2019, 13, 9880−9894

homogeneous shake and 15 min incubation at RT, the luminescent intensity was read by a plate reader (Promega). Correspondingly, the Lipofeactamine RNAiMAX (lipo) was used as control group. $N = 6$ in each loading concentration. The optimal loading concentration for each cell type (50 nM) was applied in the following cellular function assessment experiments.

Cellular Function Assessment of miNP on the Cardiovascular Cells. The function of miRNA on cell proliferation was first evaluated by the *in situ* live-cell imaging method (IncuCyte S3). In details, the hESC-CMs at 1×10^5/mL were preseeded at 6 well plate for 2 days, then the live-cell imaging initiated at the same time of miNP treatment (50 nM) by the IncuCyte at an interval of 1 h for 48 h of post-transfection. The numbers of hESC-CMs were counted at 0 and 48 h. Three replicates for two groups: miNP and miNP-scramble.

The cell proliferation was further quantitatively analyzed by the confocal images of double fluorescently immunostained Ki67 and alpha-actinin in both miNP and lipo groups, and the scrambled miRNA was included as a control group. In brief, Ki67 and alpha-actinin of hESC-CMs were fluorescently immunostained with anti-Ki67 from rabbit (ab15580, 1:100, Abcam) and anti-alpha-actinin from mouse (A7811, 1:200, Sigma), and correspondingly the secondary antibodies of Alexa Fluor donkey-antirabbit 488 and Alexa Fluor donkey-antimouse 647, followed by imaging using confocal microscopy (Carl Zeiss LSM710) with multichannels at 488 and 647 nm. DAPI was counter stained as well. Ten images at 10× magnification were taken from each replicate, and each group had 3 replicates. The hESC-CMs showing in double-positive of Ki67 and alpha-actinin were considered in cell cycle re-entry.

The activity of cell proliferation at varied loading concentration from 0 to 200 nM of miRNA was evaluated by the CellTiter 96 AQueous One Solution Cell Proliferation Assay (Promega) on the hESC-CMs, hESC-ECs and hCFs. Specifically, a mixture of 20 μL CellTiter 96 Aqueous reagent and 100 μL culture medium was added into each well of the 96-well plate after 48 h of miNP treatment. After 1.5 h of incubation in the cell culture incubator, the absorbance was recorded by a microplate reader at 490 nm ($N = 6$ in each loading concentration). The 48 h proliferation of hESC-CMs, -ECs, and hCFs treated with miNP was normalized to the untreated groups. The effect of hypoxic condition on the activity of proliferation of hESC-CM and -ECs was normalized to the proliferation in normoxic condition.

The cellular responses of miNP treatment on the transcriptional levels of hESC-CMs, hESC-ECs, and hCFs under hypoxic condition were measured by the real-time quantitative PCR (RT-qPCR). Six groups were studied: miNP in normoxia and hypoxia, miNP-scramble in normoxia and hypoxia, and control (without any treatment) in normoxia and hypoxia. First, RNA was extracted using RNeasy Mini Kit (Qiagen). All the RNAs used in this study were A260/280 = 1.9–2.1. Then 500 ng cDNA was synthesized *via* reverse transcription using the iScript cDNA Synthesis Kit (Bio-Rad). The qPCR was performed with the TaqMan gene expression assay, and the mRNA expression levels of GAPDH, CDC6, CCNE1, CDK7, AURKB, VEGFA, and HIF1A were examined. The final results were demonstrated as the relative expressions to the control group ($N = 3$ in each group).

Hydrogel Synthesis and Characterization. The engineered injectable hydrogel was synthesized and purified as previously described.[33] Briefly, the cross-linked elastin-like protein–hyaluronic acid (ELP-HA, 1 wt %/1 wt %) mixing the two components at room temperature formed hydrogel: hydrazine-modified ELP (ELP-HYD) and aldehyde-modified HA (HA-ALD). The ELP used in this study, with a molecular weight of 37840 Da, is a recombinant protein made in-house containing a bioactive cell-adhesive RGD domain. HA (M_w: 700 kDa) was purchased from Lifecore Biomedical.

Mechanical measurements were performed on a stress-controlled rheometer (ARG2, TA Instruments) using a 20 mm diameter, following cone-on-plate geometry. Samples were allowed to gel *in situ* on the rheometer, and a humidity chamber was secured in place to prevent dehydration. Gelation time sweep was performed at oscillatory stress of 4.74 Pa at 25 °C for 5 min, followed by another 5 min at 37 °C to allow full gelation and equilibrium at physiological temperature. All further measurements were made at 37 °C. A strain sweep from 0.1 to 1000% were performed at an angular frequency of 1 Hz to test the linear viscoelastic region (LVR) of the material. Angular frequency sweep was conducted from 0.1 to 10 Hz with a constant 5% strain amplitude. Shear-thinning and self-healing properties of the gel sample were characterized by measuring linear viscosity (η) under a time sweep mode at alternating low and high shear rates of 0.1 and 10 s^{-1}, respectively, for 1 min each and a total of 7 min. A stress relaxation test was conducted under a constant strain of 10%.

***In Vivo* Nanoparticle Delivery *via* Injectable Hydrogel in a Rat MI Model.** First, the subacute MI model was achieved in the RNU rats (Charles River Laboratories) *via* a 1 h ligation and reperfusion. Then, the chest was reopened and 15 μL of NP-hydrogel composite was injected intramyocardially at 3 sites at the edge of the infarct zone with a 28-gauge insulin syringe. Five experimental groups in total were studied: PBS, miNP, hydrogel, hydrogel/miNP-scramble, and hydrogel/miNP. The details of NP-hydrogel composite formation are as follows: the miNPs or miNP-scramble were encapsulated within the ELP-HA hydrogel briefly, and the 3 μL miNP or miNP-scramble stock solution was first well mixed with the ice-cold 6 μL ELP-HYD solution, followed by mixing with 6 μL HA-ALD solution to form the gel. For the hydrogel group, 3 μL miNP stock solution was replaced by 3 μL 1× PBS. For the miNP group, 3 μL miNP stock solution and 12 μL PBS were mixed before injection. For the PBS group, 15 μL PBS was used. Study protocols were approved by the Stanford Animal Research Committee. Animal care was provided in accordance with the Stanford University School of Medicine guidelines and policies for the use of laboratory animals.

Echocardiography. At −1 day, 1 and 3 months after hydrogel/miNP injection, cardiac function was evaluated by the transthoracic echocardiography (Vevo 2100 Imaging System, VisualSonics). Rats were anesthetized with 2% inhaled isoflurane, while LV internal dimensions were measured in systole and diastole using leading-edge methods and guidelines of the American Society of Echocardiography.[75] LV systolic function was quantitatively measured using the Vevo Lab software.

Histology. The rats were sacrificed at 28 days to harvest the heart. The harvested hearts were fixed with 4% (wt/v) paraformaldehyde overnight at 4 °C, and then immersed in 30% (wt/v) sucrose solution in the following 24 h at 4 °C. After embedding and frozen in the OCT, the blocks were then cryosectioned into sections at 10 μm. The slides with myocardial sections were further stained with Picro Sirius Red (ab150681, Abcam) to visualize the dense collagen fibers in the fibrotic area. Hematoxylin and eosin (H&E) staining was performed to examine the immune response and hydrogel engraftment in the myocardium.

The immunofluorescence staining was performed to identify the proliferation of CMs in the border zone of left ventricular tissue sections with ki67 (ab15580, 1:100, Abcam), cTnT (ab45932, 1:300, Abcam) and DAPI. To calculate the CM proliferation rate in the border zone, images at 10× per rat were taken in each group, the cells with double positives of ki67 and cTnT were considered proliferative CMs, and the number of rats in each group was 4. Also, the capillary in the border zone was stained with isolectin GS-IB4 Alexa Fluor 594 Conjugate (I21413, Thermo Fisher Scientific). To calculate the capillary density in the border zone, images at 10× per rat were taken in each group, and the number of rats in each group was 4.

Tube Formation Assay. The mixture of 2×10^5/mL hESC-ECs and miNP or miNP-scramble was seeded on the Matrigel (growth factor reduced; Corning) precoated 24 well plates. After cell seeding, the plate was kept in cell culture incubator with or without the BD GasPak EZ pouch systems (Becton Dickinson). In total, 6 experimental groups were included: control-normoxia, miRNA-scramble-normoxia, miRNA-normoxia, control-hypoxia, miRNA-scramble-hypoxia, miRNA-hypoxia ($N = 10–12$ per group). At 24 h, one image at 4× was taken from each group. The ImageJ plugin, Angiogenesis Analyzer, was applied to analyze the tubes. Accordingly, three parameters were selected: number of nodes, number of junctions, and number of branches.

DOI: 10.1021/acsnano.9b03343
ACS Nano 2019, 13, 9880–9894

Fibrosis Contraction Assay. First, cast the mixture of 6×10^6/mL hCFs, type I collagen at 2 mg/mL and 1 N NaOH in the 0.2% F127 (Thermo Fisher) precoated 48 well plate. After 1 h solidification in the culture incubator, 300 μL RPMI with 10% FBS medium was added to float the round cell-collagen construct. In total, 6 experimental groups were included: control-normoxia, miRNA-scramble-normoxia, miRNA-normoxia, control-hypoxia, miRNA-scramble-hypoxia, miRNA-hypoxia, and 6 replicates per group. At 24 h, one image at 4× was taken from each group. The diameter of each sample was measured, and the area of the construct was then calculated accordingly.

Statistical Analysis. Data are presented as mean ± SEM (standard error of the mean). Statistical significance was determined using either Student's *t* test or one-way ANOVA test. $P < 0.05$ was considered as significant difference. The *in vivo* results obtained from the echocardiography were double-blinded to the animal surgeon and echocardiography operator.

ASSOCIATED CONTENT

Supporting Information

The Supporting Information is available free of charge on the ACS Publications website at DOI: 10.1021/acsnano.9b03343.

Schematics of miNP synthesis; Confocal images of immunofluorescent staining of hESC-CMs and hESC-ECs; Schematic procedure of *in vivo* experiments and follow-up characterizations; Rheological characterization of injectable hydrogel; Engraftment and release of miNP in the myocardium; Vascular function and fibrosis contaction evaluation (PDF)

Video S1 (AVI)

AUTHOR INFORMATION

Corresponding Authors

*E-mail: huaxiao@stanford.edu.

*E-mail: lik@sustech.edu.cn.

ORCID

Dan Ding: 0000-0003-1873-6510

Sarah C. Heilshorn: 0000-0002-9801-6304

Kai Li: 0000-0003-1664-5439

Notes

The authors declare no competing financial interest.

ACKNOWLEDGMENTS

This publication was supported in part by the Thousand Young Talents Program (K.L.), and the National Natural Science Foundation of China 31870991 (K.L.), the American Heart Association (AHA) Postdoctoral Fellowship Award 18POST34030106 (H.Y.) and 17SDG33460212 (X.Q.), Stanford Cardiovascular Institute (CVI)/Gooter Foundation seed grant (H.Y., O.A., H.T.W.), and the National Institutes of Health R21 HL138042, R01 HL 142718 (S.C.H.), and K01 HL130608 (O.J.A.). We would like to thank Sohiel Memarsadeghi, Wesley Shipley, and Beth Harding's technical assistance from Essen BioScience on utilizing the IncuCyte S3 in the live-cell imaging experiments, and also thank Dr. Andrew Olsen from Stanford Neuroscience Microscopy Service on the support of confocal imaging of hESC derived cardiovascular cells.

REFERENCES

(1) Benjamin, E. J.; Virani, S. S.; Callaway, C. W.; Chamberlain, A. M.; Chang, A. R.; Cheng, S.; Chiuve, S. E.; Cushman, M.; Delling, F. N.; Deo, R.; de Ferranti, S. D.; Ferguson, J. F.; Fornage, M.; Gillespie, C.; Isasi, C. R.; Jimenez, M. C.; Jordan, L. C.; Judd, S. E.; Lackland, D.; Lichtman, J. H.; et al. Heart Disease and Stroke Statistics-2018 Update: A Report from the American Heart Association. *Circulation* **2018**, *137*, e67−e492.

(2) Anderson, J. L.; Morrow, D. A. Acute Myocardial Infarction. *N. Engl. J. Med.* **2017**, *376*, 2053−2064.

(3) El-Battrawy, I.; Borggrefe, M.; Akin, I. Beta-Blockers and Outcome after Acute Myocardial Infarction. *J. Am. Coll. Cardiol.* **2017**, *70*, 1685.

(4) Maniwa, N.; Fujino, M.; Nakai, M.; Nishimura, K.; Miyamoto, Y.; Kataoka, Y.; Asaumi, Y.; Tahara, Y.; Nakanishi, M.; Anzai, T.; Kusano, K.; Akasaka, T.; Goto, Y.; Noguchi, T.; Yasuda, S. Anticoagulation Combined with Antiplatelet Therapy in Patients with Left Ventricular Thrombus after First Acute Myocardial Infarction. *Eur. Heart J.* **2018**, *39*, 201−208.

(5) Serban, M. C.; Colantonio, L. D.; Manthripragada, A. D.; Monda, K. L.; Bittner, V. A.; Banach, M.; Chen, L.; Huang, L.; Dent, R.; Kent, S. T.; Muntner, P.; Rosenson, R. S. Statin Intolerance and Risk of Coronary Heart Events and All-Cause Mortality Following Myocardial Infarction. *J. Am. Coll. Cardiol.* **2017**, *69*, 1386−1395.

(6) Shiba, Y.; Gomibuchi, T.; Seto, T.; Wada, Y.; Ichimura, H.; Tanaka, Y.; Ogasawara, T.; Okada, K.; Shiba, N.; Sakamoto, K.; Ido, D.; Shiina, T.; Ohkura, M.; Nakai, J.; Uno, N.; Kazuki, Y.; Oshimura, M.; Minami, I.; Ikeda, U. Allogeneic Transplantation of iPS Cell-Derived Cardiomyocytes Regenerates Primate Hearts. *Nature* **2016**, *538*, 388−391.

(7) Chong, J. J.; Yang, X.; Don, C. W.; Minami, E.; Liu, Y. W.; Weyers, J. J.; Mahoney, W. M.; Van Biber, B.; Cook, S. M.; Palpant, N. J.; Gantz, J. A.; Fugate, J. A.; Muskheli, V.; Gough, G. M.; Vogel, K. W.; Astley, C. A.; Hotchkiss, C. E.; Baldessari, A.; Pabon, L.; Reinecke, H. Human Embryonic-Stem-Cell-Derived Cardiomyocytes Regenerate Non-Human Primate Hearts. *Nature* **2014**, *510*, 273−277.

(8) Cambria, E.; Pasqualini, F. S.; Wolint, P.; Gunter, J.; Steiger, J.; Bopp, A.; Hoerstrup, S. P.; Emmert, M. Y. Translational Cardiac Stem Cell Therapy: Advancing from First-Generation to Next-Generation Cell Types. *NPJ. Regen. Med.* **2017**, *2*, 17.

(9) Behfar, A.; Crespo-Diaz, R.; Terzic, A.; Gersh, B. J. Cell Therapy for Cardiac Repair-Lessons from Clinical Trials. *Nat. Rev. Cardiol.* **2014**, *11*, 232−246.

(10) Pandey, R.; Velasquez, S.; Durrani, S.; Jiang, M.; Neiman, M.; Crocker, J. S.; Benoit, J. B.; Rubinstein, J.; Paul, A.; Ahmed, R. P. MicroRNA-1825 Induces Proliferation of Adult Cardiomyocytes and Promotes Cardiac Regeneration Post Ischemic Injury. *Am. J. Transl. Res.* **2017**, *9*, 3120−3137.

(11) Hodgkinson, C. P.; Kang, M. H.; Dal-Pra, S.; Mirotsou, M.; Dzau, V. J. MicroRNAs and Cardiac Regeneration. *Circ. Res.* **2015**, *116*, 1700−1711.

(12) Porrello, E. R.; Johnson, B. A.; Aurora, A. B.; Simpson, E.; Nam, Y. J.; Matkovich, S. J.; Dorn, G. W., 2nd; van Rooij, E.; Olson, E. N. MiR-15 Family Regulates Postnatal Mitotic Arrest of Cardiomyocytes. *Circ. Res.* **2011**, *109*, 670−679.

(13) Witman, N.; Heigwer, J.; Thaler, B.; Lui, W. O.; Morrison, J. I. miR-128 Regulates Non-Myocyte Hyperplasia, Deposition of Extracellular Matrix and Islet1 Expression during Newt Cardiac Regeneration. *Dev. Biol.* **2013**, *383*, 253−263.

(14) Tian, Y.; Liu, Y.; Wang, T.; Zhou, N.; Kong, J.; Chen, L.; Snitow, M.; Morley, M.; Li, D.; Petrenko, N.; Zhou, S.; Lu, M.; Gao, E.; Koch, W. J.; Stewart, K. M.; Morrisey, E. E. A microRNA-Hippo Pathway That Promotes Cardiomyocyte Proliferation and Cardiac Regeneration in Mice. *Sci. Transl. Med.* **2015**, *7*, 279ra38−279ra38.

(15) Lesizza, P.; Prosdocimo, G.; Martinelli, V.; Sinagra, G.; Zacchigna, S.; Giacca, M. Single-Dose Intracardiac Injection of Pro-Regenerative MicroRNAs Improves Cardiac Function after Myocardial Infarction. *Circ. Res.* **2017**, *120*, 1298−1304.

(16) Eulalio, A.; Mano, M.; Dal Ferro, M.; Zentilin, L.; Sinagra, G.; Zacchigna, S.; Giacca, M. Functional Screening Identifies MiRNAs Inducing Cardiac Regeneration. *Nature* **2012**, *492*, 376−381.

(17) Shatseva, T.; Lee, D. Y.; Deng, Z.; Yang, B. B. MicroRNA miR-199a-3p Regulates Cell Proliferation and Survival by Targeting Caveolin-2. *J. Cell Sci.* **2011**, *124*, 2826−2836.
(18) Park, K. M.; Teoh, J. P.; Wang, Y.; Broskova, Z.; Bayoumi, A. S.; Tang, Y.; Su, H.; Weintraub, N. L.; Kim, I. M. Carvedilol-Responsive MicroRNAs, miR-199a-3p and −214 Protect Cardiomyocytes from Simulated Ischemia-Reperfusion Injury. *Am. J. Physiol. Heart Circ. Physiol.* **2016**, *311*, H371−H383.
(19) Savary, G.; Dewaeles, E.; Diazzi, S.; Buscot, M.; Nottet, N.; Fassy, J.; Courcot, E.; Henaoui, I. S.; Lemaire, J.; Martis, N.; Van der Hauwaert, C.; Pons, N.; Magnone, V.; Leroy, S.; Hofman, V.; Plantier, L.; Lebrigand, K.; Paquet, A.; Lino Cardenas, C. L.; Vassaux, G.; et al. The Long Non-Coding RNA DNM3OS is a reservoir of FibromiRs with Major Functions in Lung Fibroblast Response to TGF-Beta and Pulmonary Fibrosis. *Am. J. Respir. Crit. Care Med.* **2019**, DOI: 10.1164/rccm.201807-1237OC.
(20) Mak, K. Y.; Rajapaksha, I. G.; Angus, P. W.; Herath, C. B. The Adeno-associated Virus - A Safe and Promising Vehicle for Liverspecific Gene Therapy of Inherited and Non-inherited Disorders. *Curr. Gene Ther.* **2017**, *17*, 4−16.
(21) Corti, M.; Liberati, C.; Smith, B. K.; Lawson, L. A.; Tuna, I. S.; Conlon, T. J.; Coleman, K. E.; Islam, S.; Herzog, R. W.; Fuller, D. D.; Collins, S. W.; Byrne, B. J. Safety of Intradiaphragmatic Delivery of Adeno-Associated Virus-Mediated Alpha-Glucosidase (rAAV1-CMV-hGAA) Gene Therapy in Children Affected by Pompe Disease. *Hum. Gene Ther.: Clin. Dev.* **2017**, *28*, 208−218.
(22) Prosdocimo, G. Development of The Clinical Application of miRNA with Proregenerative Effect on The Heart. Thesis (PhD), The Open University, 2018.
(23) Malam, Y.; Loizidou, M.; Seifalian, A. M. Liposomes and Nanoparticles: Nanosized Vehicles for Drug Delivery in Cancer. *Trends Pharmacol. Sci.* **2009**, *30*, 592−599.
(24) Chen, J.; Guo, Z.; Tian, H.; Chen, X. Production and Clinical Development of Nanoparticles for Gene Delivery. *Mol. Ther.–Methods Clin. Dev.* **2016**, *3*, 16023.
(25) Zylberberg, C.; Gaskill, K.; Pasley, S.; Matosevic, S. Engineering Liposomal Nanoparticles for Targeted Gene Therapy. *Gene Ther.* **2017**, *24*, 441−452.
(26) Djurovic, S.; Iversen, N.; Jeansson, S.; Hoover, F.; Christensen, G. Comparison of Nonviral Transfection and Adeno-Associated Viral Transduction on Cardiomyocytes. *Mol. Biotechnol.* **2004**, *28*, 21−32.
(27) Xue, X.; Shi, X.; Dong, H.; You, S.; Cao, H.; Wang, K.; Wen, Y.; Shi, D.; He, B.; Li, Y. Delivery of microRNA-1 Inhibitor by Dendrimer-based Nanovector: An Early Targeting Therapy for Myocardial Infarction in Mice. *Nanomedicine* **2018**, *14*, 619−631.
(28) Qin, X.; Chen, H.; Yang, H.; Wu, H.; Zhao, X.; Wang, H.; Chour, T.; Neofytou, E.; Ding, D.; Daldrup-Link, H.; Heilshorn, S. C.; Li, K.; Wu, J. C. Photoacoustic Imaging of Embryonic Stem Cell-Derived Cardiomyocytes in Living Hearts with Ultrasensitive Semiconducting Polymer Nanoparticles. *Adv. Funct. Mater.* **2018**, *28*, 1704939.
(29) Waters, R.; Alam, P.; Pacelli, S.; Chakravarti, A. R.; Ahmed, R. P. H.; Paul, A. Stem Cell-inspired Secretome-Rich Injectable Hydrogel to Repair Injured Cardiac Tissue. *Acta Biomater.* **2018**, *69*, 95−106.
(30) Wang, T.; Wu, D. Q.; Jiang, X. J.; Zhang, X. Z.; Li, X. Y.; Zhang, J. F.; Zheng, Z. B.; Zhuo, R.; Jiang, H.; Huang, C. Novel Thermosensitive Hydrogel Injection Inhibits Post-Infarct Ventricle Remodelling. *Eur. J. Heart Failure* **2009**, *11*, 14−19.
(31) Suarez, S. L.; Rane, A. A.; Munoz, A.; Wright, A. T.; Zhang, S. X.; Braden, R. L.; Almutairi, A.; McCulloch, A. D.; Christman, K. L. Intramyocardial Injection of Hydrogel with High Interstitial Spread Does Not Impact Action Potential Propagation. *Acta Biomater.* **2015**, *26*, 13−22.
(32) Nelson, D. M.; Ma, Z.; Fujimoto, K. L.; Hashizume, R.; Wagner, W. R. Intra-Myocardial Biomaterial Injection Therapy in The Treatment of Heart Failure: Materials, Outcomes and Challenges. *Acta Biomater.* **2011**, *7*, 1−15.
(33) Wang, H. Y.; Zhu, D. Q.; Paul, A.; Cai, L.; Enejder, A.; Yang, F.; Heilshorn, S. C. Covalently Adaptable Elastin-Like Protein-Hyaluronic Acid (ELP-HA) Hybrid Hydrogels with Secondary Thermoresponsive Crosslinking for Injectable Stem Cell Delivery. *Adv. Funct. Mater.* **2017**, *27*, 1605609.
(34) Steele, A. N.; Cai, L.; Truong, V. N.; Edwards, B. B.; Goldstone, A. B.; Eskandari, A.; Mitchell, A. C.; Marquardt, L. M.; Foster, A. A.; Cochran, J. R.; Heilshorn, S. C.; Woo, Y. J. A Novel Protein-engineered Hepatocyte Growth Factor Analog Released *via* A Shear-Thinning Injectable Hydrogel Enhances Post-Infarction Ventricular Function. *Biotechnol. Bioeng.* **2017**, *114*, 2379−2389.
(35) Zhu, D.; Wang, H.; Trinh, P.; Heilshorn, S. C.; Yang, F. Elastin-Like Protein-Hyaluronic Acid (ELP-HA) Hydrogels with Decoupled Mechanical and Biochemical Cues for Cartilage Regeneration. *Biomaterials* **2017**, *127*, 132−140.
(36) Jin, G.; Mao, D.; Cai, P.; Liu, R.; Tomczak, N.; Liu, J.; Chen, X.; Kong, D.; Ding, D.; Liu, B.; Li, K. Conjugated Polymer Nanodots As Ultrastable Long-Term Trackers to Understand Mesenchymal Stem Cell Therapy in Skin Regeneration. *Adv. Funct. Mater.* **2015**, *25*, 4263−4273.
(37) Jin, G.; Feng, G.; Qin, W.; Tang, B. Z.; Liu, B.; Li, K. Multifunctional Organic Nanoparticles with Aggregation-Induced Emission (AIE) Characteristics for Targeted Photodynamic Therapy and RNA Interference Therapy. *Chem. Commun.* **2016**, *52*, 2752−2755.
(38) Ghosh, S.; Pulinilkunnil, T.; Yuen, G.; Kewalramani, G.; An, D.; Qi, D.; Abrahani, A.; Rodrigues, B. Cardiomyocyte Apoptosis Induced by Short-Term Diabetes Requires Mitochondrial GSH Depletion. *Am. J. Physiol. Heart Circ. Physiol.* **2005**, *289*, H768−H776.
(39) Zhao, M. T.; Chen, H.; Liu, Q.; Shao, N. Y.; Sayed, N.; Wo, H. T.; Zhang, J. Z.; Ong, S. G.; Liu, C.; Kim, Y.; Yang, H.; Chour, T.; Ma, H.; Gutierrez, N. M.; Karakikes, I.; Mitalipov, S.; Snyder, M. P.; Wu, J. C. Molecular and Functional Resemblance of Differentiated Cells Derived from Isogenic Human iPSCs and SCNT-Derived ESCs. *Proc. Natl. Acad. Sci. U. S. A.* **2017**, *114*, E11111−E11120.
(40) Sayed, N.; Liu, C.; Wu, J. C. Translation of Human-Induced Pluripotent Stem Cells: From Clinical Trial in A Dish to Precision Medicine. *J. Am. Coll. Cardiol.* **2016**, *67*, 2161−2176.
(41) Tian, Y.; Liu, Y.; Wang, T.; Zhou, N.; Kong, J.; Chen, L.; Snitow, M.; Morley, M.; Li, D. Q.; Petrenko, N.; Zhou, S.; Lu, M. M.; Gao, E. H.; Koch, W. J.; Stewart, K. M.; Morrisey, E. E. A MicroRNA-Hippo Pathway That Promotes Cardiomyocyte Proliferation and Cardiac Regeneration in Mice. *Sci. Transl. Med.* **2015**, *7*, 279ra38.
(42) Valdmanis, P. N.; Kay, M. A. Future of rAAV Gene Therapy: Platform for RNAi, Gene Editing, and Beyond. *Hum. Gene Ther.* **2017**, *28*, 361−372.
(43) Janas, M. M.; Jiang, Y.; Schlegel, M. K.; Waldron, S.; Kuchimanchi, S.; Barros, S. A. Impact of Oligonucleotide Structure, Chemistry, and Delivery Method on *In Vitro* Cytotoxicity. *Nucleic Acid Ther.* **2017**, *27*, 11−22.
(44) Li, K.; Liu, B. Polymer-encapsulated Organic Nanoparticles for Fluorescence and Photoacoustic Imaging. *Chem. Soc. Rev.* **2014**, *43*, 6570−6597.
(45) Musacchio, T.; Vaze, O.; D'Souza, G.; Torchilin, V. P. Effective Stabilization and Delivery of siRNA: Reversible siRNA-Phospholipid Conjugate in Nanosized Mixed Polymeric Micelles. *Bioconjugate Chem.* **2010**, *21*, 1530−1536.
(46) De Jong, W. H.; Borm, P. J. Drug Delivery and Nanoparticles: Applications and Hazards. *Int. J. Nanomed.* **2008**, *3*, 133−149.
(47) Jiang, J. K.; Oberdorster, G.; Biswas, P. Characterization of Size, Surface Charge, and Agglomeration State of Nanoparticle Dispersions for Toxicological Studies. *J. Nanopart. Res.* **2009**, *11*, 77−89.
(48) Abilez, O. J.; Tzatzalos, E.; Yang, H.; Zhao, M. T.; Jung, G.; Zollner, A. M.; Tiburcy, M.; Riegler, J.; Matsa, E.; Shukla, P.; Zhuge, Y.; Chour, T.; Chen, V. C.; Burridge, P. W.; Karakikes, I.; Kuhl, E.; Bernstein, D.; Couture, L. A.; Gold, J. D.; Zimmermann, W. H. Passive Stretch Induces Structural and Functional Maturation of Engineered Heart Muscle as Predicted by Computational Modeling. *Stem Cells* **2018**, *36*, 265−277.

DOI: 10.1021/acsnano.9b03343
ACS Nano 2019, 13, 9880−9894

(49) Guan, Y.; Xu, D.; Garfin, P. M.; Ehmer, U.; Hurwitz, M.; Enns, G.; Michie, S.; Wu, M.; Zheng, M.; Nishimura, T.; Sage, J.; Peltz, G. Human Hepatic Organoids for The Analysis of Human Genetic Diseases. *JCI Insight* **2017**, *2*, No. e94954.
(50) Pasca, A. M.; Sloan, S. A.; Clarke, L. E.; Tian, Y.; Makinson, C. D.; Huber, N.; Kim, C. H.; Park, J. Y.; O'Rourke, N. A.; Nguyen, K. D.; Smith, S. J.; Huguenard, J. R.; Geschwind, D. H.; Barres, B. A.; Pasca, S. P. Functional Cortical Neurons and Astrocytes from Human Pluripotent Stem Cells in 3D Culture. *Nat. Methods* **2015**, *12*, 671−678.
(51) Burridge, P. W.; Matsa, E.; Shukla, P.; Lin, Z. C.; Churko, J. M.; Ebert, A. D.; Lan, F.; Diecke, S.; Huber, B.; Mordwinkin, N. M.; Plews, J. R.; Abilez, O. J.; Cui, B.; Gold, J. D.; Wu, J. C. Chemically Defined Generation of Human Cardiomyocytes. *Nat. Methods* **2014**, *11*, 855−860.
(52) Zhao, X.; Chen, H.; Xiao, D.; Yang, H.; Itzhaki, I.; Qin, X.; Chour, T.; Aguirre, A.; Lehmann, K.; Kim, Y.; Shukla, P.; Holmstrom, A.; Zhang, J. Z.; Zhuge, Y.; Ndoye, B. C.; Zhao, M.; Neofytou, E.; Zimmermann, W. H.; Jain, M.; Wu, J. C. Comparison of Non-Human Primate *versus* Human Induced Pluripotent Stem Cell-Derived Cardiomyocytes for Treatment of Myocardial Infarction. *Stem Cell Rep.* **2018**, *10*, 422−435.
(53) Shadrin, I. Y.; Allen, B. W.; Qian, Y.; Jackman, C. P.; Carlson, A. L.; Juhas, M. E.; Bursac, N. Cardiopatch Platform Enables Maturation and Scale-Up of Human Pluripotent Stem Cell-derived Engineered Heart Tissues. *Nat. Commun.* **2017**, *8*, 1825.
(54) Weinberger, F.; Mannhardt, I.; Eschenhagen, T. Engineering Cardiac Muscle Tissue: A Maturating Field of Research. *Circ. Res.* **2017**, *120*, 1487−1500.
(55) Cai, K. M.; He, X.; Song, Z. Y.; Yin, Q.; Zhang, Y. F.; Uckun, F. M.; Jiang, C.; Cheng, J. J. Dimeric Drug Polymeric Nanoparticles with Exceptionally High Drug Loading and Quantitative Loading Efficiency. *J. Am. Chem. Soc.* **2015**, *137*, 3458−3461.
(56) Hodne, K.; Lipsett, D. B.; Louch, W. E. Gene Transfer in Isolated Adult Cardiomyocytes. *Methods Mol. Biol.* **2017**, *1521*, 169−182.
(57) Guidotti, G.; Brambilla, L.; Rossi, D. Cell-Penetrating Peptides: From Basic Research to Clinics. *Trends Pharmacol. Sci.* **2017**, *38*, 406−424.
(58) Josephson, L.; Tung, C. H.; Moore, A.; Weissleder, R. High-Efficiency Intracellular MagneticLabeling with Novel Superparamagnetic-Tat Peptide Conjugates. *Bioconjugate Chem.* **1999**, *10*, 186−191.
(59) Sievers, R. E.; Schmiedl, U.; Wolfe, C. L.; Moseley, M. E.; Parmley, W. W.; Brasch, R. C.; Lipton, M. J. A Model of Acute Regional Myocardial Ischemia and Reperfusion in The Rat. *Magn. Reson. Med.* **1989**, *10*, 172−181.
(60) Sutton, M. G.; Sharpe, N. Left Ventricular Remodeling After Myocardial Infarction: Pathophysiology and Therapy. *Circulation* **2000**, *101*, 2981−2988.
(61) Oka, T.; Akazawa, H.; Naito, A. T.; Komuro, I. Angiogenesis and Cardiac Hypertrophy: Maintenance of Cardiac Function and Causative Roles in Heart Failure. *Circ. Res.* **2014**, *114*, 565−571.
(62) Gu, M.; Shao, N. Y.; Sa, S.; Li, D.; Termglinchan, V.; Ameen, M.; Karakikes, I.; Sosa, G.; Grubert, F.; Lee, J.; Cao, A.; Taylor, S.; Ma, Y.; Zhao, Z.; Chappell, J.; Hamid, R.; Austin, E. D.; Gold, J. D.; Wu, J. C.; Snyder, M. P. Patient-Specific iPSC-Derived Endothelial Cells Uncover Pathways That Protect Against Pulmonary Hypertension in BMPR2Mutation Carriers. *Cell Stem Cell* **2017**, *20*, 490−504.
(63) Kodo, K.; Ong, S. G.; Jahanbani, F.; Termglinchan, V.; Hirono, K.; InanlooRahatloo, K.; Ebert, A. D.; Shukla, P.; Abilez, O. J.; Churko, J. M.; Karakikes, I.; Jung, G.; Ichida, F.; Wu, S. M.; Snyder, M. P.; Bernstein, D.; Wu, J. C. iPSC-Derived Cardiomyocytes Reveal Abnormal TGF-Beta Signalling in Left Ventricular Non-Compaction Cardiomyopathy. *Nat. Cell Biol.* **2016**, *18*, 1031−1042.
(64) Sayed, N.; Wu, J. C. Towards Cardio-Precision medicine. *Eur. Heart J.* **2017**, *38*, 1014−1016.
(65) Piatti, S.; Lengauer, C.; Nasmyth, K. Cdc6 Is An Unstable Protein Whose De Novo Synthesis in G1 Is Important for The Onset of S Phase and for Preventing A 'Reductional' Anaphase in The Budding Yeast Saccharomyces Cerevisiae. *EMBO J.* **1995**, *14*, 3788−3799.
(66) Mohamed, T. M. A.; Ang, Y. S.; Radzinsky, E.; Zhou, P.; Huang, Y.; Elfenbein, A.; Foley, A.; Magnitsky, S.; Srivastava, D. Regulation of Cell Cycle to Stimulate Adult Cardiomyocyte Proliferation and Cardiac Regeneration. *Cell* **2018**, *173*, 104−116.
(67) Gaengel, K.; Genove, G.; Armulik, A.; Betsholtz, C. Endothelial-Mural Cell Signaling in Vascular Development and Angiogenesis. *Arterioscler., Thromb., Vasc. Biol.* **2009**, *29*, 630−638.
(68) Zhu, W.; Zhao, M.; Mattapally, S.; Chen, S.; Zhang, J. CCND2 Overexpression Enhances The Regenerative Potency of Human Induced Pluripotent Stem Cell-Derived Cardiomyocytes: Remuscularization of Injured Ventricle. *Circ. Res.* **2018**, *122*, 88−96.
(69) Kishida, N.; Maki, T.; Takagi, Y.; Yasuda, K.; Kinoshita, H.; Ayaki, T.; Noro, T.; Kinoshita, Y.; Ono, Y.; Kataoka, H.; Yoshida, K.; Lo, E. H.; Arai, K.; Miyamoto, S.; Takahashi, R. Role of Perivascular Oligodendrocyte Precursor Cells in Angiogenesis After Brain Ischemia. *J. Am. Heart Assoc.* **2019**, *8*, No. e011824.
(70) Hubbi, M. E.; Semenza, G. L. Regulation of Cell Proliferation by Hypoxia-Inducible Factors. *A. J. Physiol. Cell Ph.* **2015**, *309*, C775−C782.
(71) Licht, A. H.; Muller-Holtkamp, F.; Flamme, I.; Breier, G. Inhibition of Hypoxia-Inducible Factor Activity in Endothelial Cells Disrupts Embryonic Cardiovascular Development. *Blood* **2006**, *107*, 584−590.
(72) Semenza, G. L. Hypoxia-Inducible Factor 1 and Cardiovascular Disease. *Annu. Rev. Physiol.* **2014**, *76*, 39−56.
(73) Tao, Z.; Chen, B.; Tan, X.; Zhao, Y.; Wang, L.; Zhu, T.; Cao, K.; Yang, Z.; Kan, Y. W.; Su, H. Coexpression of VEGF and Angiopoietin-1 Promotes Angiogenesis and Cardiomyocyte Proliferation Reduces Apoptosis in Porcine Myocardial Infarction (MI) Heart. *Proc. Natl. Acad. Sci. U. S. A.* **2011**, *108*, 2064−2069.
(74) Guimaraes-Camboa, N.; Stowe, J.; Aneas, I.; Sakabe, N.; Cattaneo, P.; Henderson, L.; Kilberg, M. S.; Johnson, R. S.; Chen, J.; McCulloch, A. D.; Nobrega, M. A.; Evans, S. M.; Zambon, A. C. HIF1alpha Represses Cell Stress Pathways to Allow Proliferation of Hypoxic Fetal Cardiomyocytes. *Dev. Cell* **2015**, *33*, 507−521.
(75) Sahn, D. J.; DeMaria, A.; Kisslo, J.; Weyman, A. Recommendations Regarding Quantitation in M-Mode Echocardiography: Results of A Survey of Echocardiographic Measurements. *Circulation* **1978**, *58*, 1072−1083.

DOI: 10.1021/acsnano.9b03343
ACS Nano 2019, 13, 9880−9894